

Chapter 1

Phenomena of Perturbation in Electrical Systems

1.1. Electromagnetic perturbations in energy systems

1.1.1. Introduction

Power electronic systems are increasingly being used in every field; initially, they were used in the industrial sector and then used increasingly in transportation, services and housing sectors. The flexibility in the control of electrical energy explains this evolution well.

For the purposes of illustration, we estimate that the electrification of service or control functions in an aircraft offers the following gains¹:

- 10% on the mass;
- 9% on fuel consumption;
- 13% on thrust from the engines;
- 15% on maintenance costs;
- 10% on the buying price.

¹ According to SAFRAN company, symposium SPEC 2007.

The field of automobiles is also subject to this evolution: the development of hybrid vehicles over the last 10 years and, more recently, the re-emergence of the fully electric car (while waiting for fuel cells vehicles) are evidence of this. Already, a large number of services have been electrified in thermal engine automobiles because of the flexibility of controls (speed variation) and high yield of the electrical systems: power steering, anti-blocking system (ABS), various pumps, window winders, air conditioning (to come).

The introduction of this technology, as a consequence, must take into consideration its implementation constraints; electromagnetic compatibility (EMC) in particular. Indeed, static converters based on power electronics are important sources of electromagnetic perturbations that can occasionally cause malfunctions in their local or distant electronic environment: avionics, navigation systems, reception antennae, etc. Thus, it is important to understand the origin of these phenomena, their mode of propagation and the effects on their potential “victims” in order to optimize the essential reduction or protection devices necessary to conform to the standards of EMC.

A chain of management of the electrical energy is generally organized according to the diagram in Figure 1.1: a primary electrical source powers the energy conversion system (distributed control), which itself powers one or more passive loads or actuators. The link between these components is achieved through conductors or power cables. The converter can itself be a complex device with different levels of conversion and have auxiliary supplies.

The converters carrying out the *processing of electrical energy* (conditioning, control) are based on the use of power electronics in the same manner as microelectronics and *signal processing*. It is noteworthy to observe that these two fields are based on the switching of semiconductors. In the first case, this involves power components (insulated grid

bipolar transistor (IGBT), metal oxide silicon field effect transistor (MOSFET, diodes, etc.)) operating with vertical conduction which, in a switching system, confer a very high efficiency to the static converters where they are used; in the other case, this involves heavily integrated lateral components that enable the increase in speed of information processing. In each case, the high-frequency operation of these systems causes electromagnetic perturbations, the disturbance frequencies of which get closer and closer.

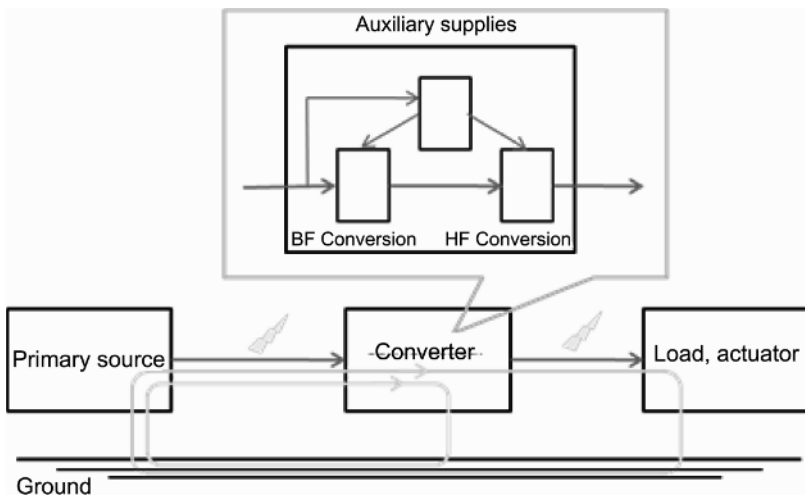


Figure 1.1. *Organization of a power electronics management system*

The consequences of the perturbations emitted by the power devices can be very serious in terms of the reliability and/or security of systems: in an airplane where security depends on electronic localization, communication and flight control systems, the introduction of electrical energy control systems based on power electronics must not threaten the current level of security; a good knowledge of these phenomena is therefore essential in this field.

Near-field or radiative couplings are proportional to the temporal derivative of the electrical quantities: Mdi/dt ,

CdV/dt ; therefore, as their importance increases, these quantities are naturally bigger and the harmonics of the commuted electrical quantities are of a higher frequency.

Thus, the switching of power semiconductors can cause conducted and emitted electromagnetic perturbations that cover a very large frequency range as shown in Figure 1.2.

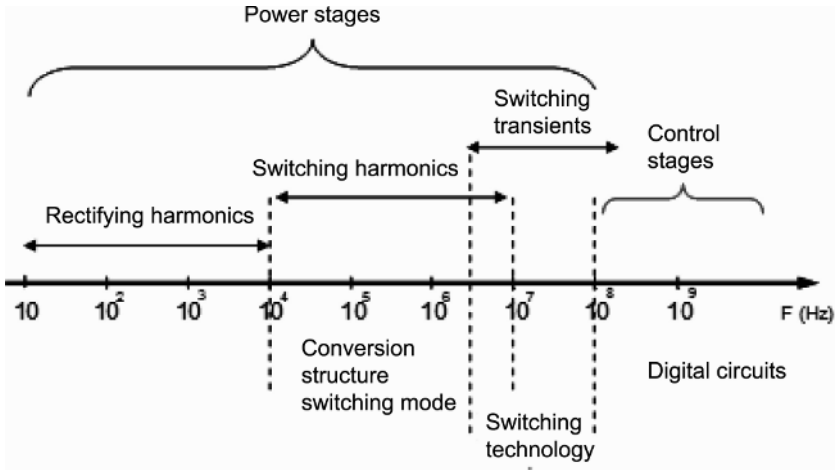


Figure 1.2. Frequency range of power electronics perturbations

– At low frequency from the network frequency of 50 Hz: the direct switching of diode or thyristor rectifiers, of triac dimmers, in synchronization with the network frequency, generates perturbations observable up to a few tens of kilohertz. This range is known as the “power grid harmonics”.

– At medium frequency (ranging from 10 kHz to 10 MHz): the switching of controlled semiconductors (MOSFET, IGBT) is performed in this range for switched-mode power supplies, choppers and power inverters. The commuted quantities show very quick temporal variations (of the order of a few 10 kV/ μ s and a few 100 A/ μ s) with extremely large spectral

contents observed over at least four frequency decades: from 10^4 to 10^8 Hz.

– At high frequency: the transients in switching of semiconductors excite the normal modes of very low resistance electrical circuits (necessary for small losses). Thus, very high frequency resonances appear (10 MHz–1 GHz) during each switching between the parasitic inductances of connections (or of magnetic components) and the structural capacitances of the semiconductors.

The reality is more complex than this first classification because in an electronic power device, there are generally several stages of conversion operating at different frequencies (rectifier, high frequency (HF) switch-mode for auxiliary power supplies, medium frequency (MF) switch-mode for power, etc.) that interfere or intermodulate. For illustrative purposes, Figure 1.3 shows the spectrum of the current measured at the input of an upstream switch-mode power supply (black curve) and at the input of a downstream rectifier (gray curve). We can clearly see the contribution of the rectifier starting from 50 Hz and the multiple harmonic peaks that it generates until approximately 10 kHz. Beyond that, we observe (black curve) multiple 15 kHz peaks (switch-mode frequency) that are modulated by the operation of the rectifier and are not modulated on the gray line: the effect of modulation is represented by a certain level of noise at the bottom of the switch-mode harmonic peaks (area circled in dotted line).

These observations show that the electromagnetic perturbations caused by the static converters are not only conducted in the electrical networks and in the cables linking the loads, but are also very easily transmitted by direct radiation, taking into account the amplitudes of the currents and voltages that are in play as well as their frequencies (see Figure 1.1).

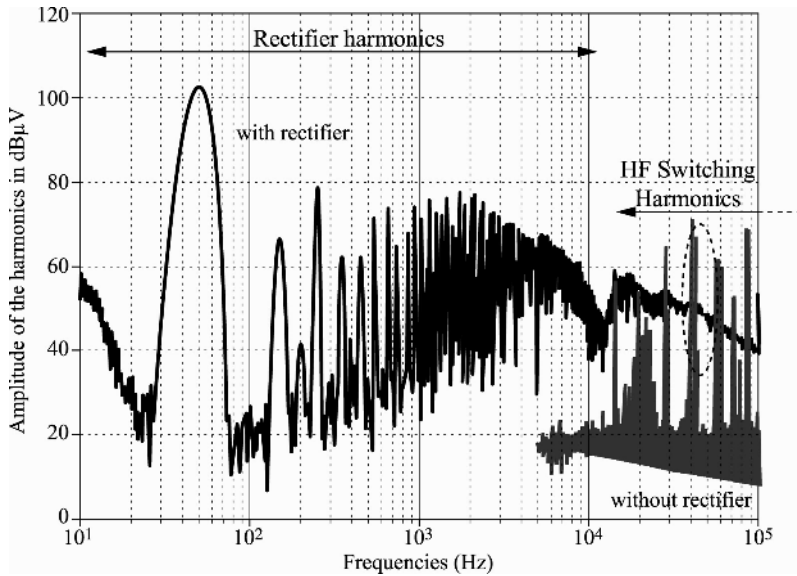


Figure 1.3. *Spectrum of parasite input current of a power supply modulated or not by the input rectifier*

1.2. Power grid harmonics

1.2.1 Presentation

In land-based or on-board (aircraft, vessels, etc.) electrical networks, the real shape of the current or voltage wave is never perfectly sinusoidal; real waves include harmonics caused by connected devices and present nonlinear features: diode rectifiers, inductive loads whose magnetic material is saturated over the course of its operation cycle (ballast of fluorescent tubes for example). They therefore summon non-sinusoidal currents which create deformations in the voltage which will, all the while remaining periodic, be deformed by harmonics, generally of odd order.

Figure 1.4 illustrates the propagation mechanism of harmonics in a grid: a nonlinear load creates harmonic currents that, while they travel through the branches of an

impedant network, create harmonic voltage drops. The voltage wave is therefore deformed at the observed points. This deformation is evidently bigger as the impedance of the network is also bigger.

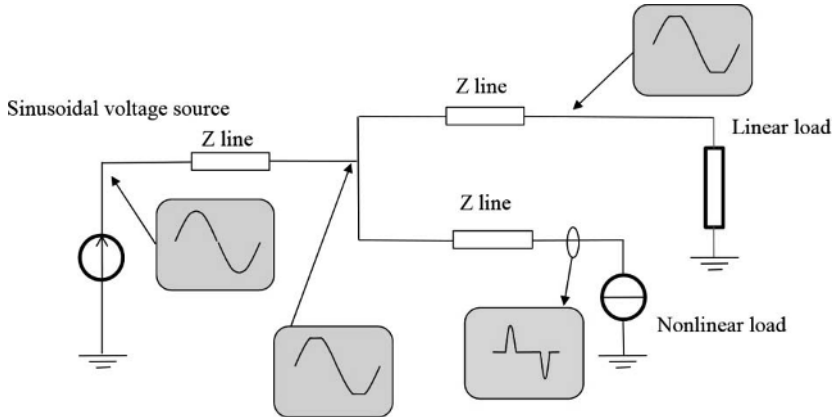


Figure 1.4. Propagation of harmonics in a network and its consequences on the voltage waveforms

In addition to the effects resulting from the flow of harmonic currents in the lines of non-zero impedance, the voltage harmonics originate from small imperfections of construction (asymmetries) in the winding of equipment, in other words, rotating machines (motors and alternators) and transformers. These third-order harmonic voltages play a small part, and with low rates, in the origin of the overall harmonic distortions.

For household appliances, it is the accumulation of devices, all in phase and connected to an insufficiently small line impedance, that creates a major harmonic pollution of the network. We can cite, for example, the simultaneous operation of multimedia devices (and of their switch-mode power supply), the constant connection of computers as well as the general use of fluorescent lamps.

The harmonics, being caused by nonlinear loads, are therefore preferentially propagated between phase and neutral on a single-phase network or between the phases of a three-phase network (supposing the load does not have a neutral connection). This is called differential-mode propagation.

1.2.2. Characterization of the quality of electrical energy

This pollution is characterized by the *total harmonic distortion* defined either by its relation to the voltage fundamental or by its relation to its root mean square (RMS), as such:

$$\text{TDH}_{\text{fund}} = \frac{\sqrt{\sum_{n=2}^{\infty} U_n^2}}{U_1} \quad \text{TDH}_{\text{RMS}} = \frac{\sqrt{\sum_{n=2}^{\infty} U_{n\text{eff}}^2}}{U_{\text{eff}}} \quad [1.1]$$

Thus, it is appropriate to be vigilant with the adopted definition when we want to quantify these effects.

Currently in France, the distortion rate, except in certain rare cases, is between:

- 5% and 8% in the low-voltage grid;
- 5% and 7% in the medium-voltage grid;
- 2% and 3% in the high-voltage grid.

The current absorbed by a nonlinear load is defined in the same way by its current distortion rate (we can also find the definition relative to the total RMS value):

$$\text{TDH}_{\text{fund}} = \frac{\sqrt{I_2^2 + I_3^2 + \dots}}{I_1} \quad [1.2]$$

Therefore, we acknowledge that the presence of harmonics contributes to the augmentation of the RMS current, which

generally increases losses (joules) in powered loads and in power lines:

$$I = \sqrt{I_1^2 + I_2^2 + I_3^2 + \dots} = I_1 \sqrt{1 + TDH_{fund}^2} \quad [1.3]$$

The quality of the electrical energy is characterized by the *power factor*, defined as the relation between the active power provided to a load and the apparent power, the product of the RMS of voltage and current. In a pure sinusoidal system, ideally the power factor tends toward 1. If we take the case of equipment powered by a purely sinusoidal single-phase voltage and absorbing a non-sinusoidal current, the power factor (per phase) in this scenario is equal to:

$$\lambda = \frac{P}{S} = \frac{V I_1 \cos \varphi_1}{V I} = \frac{1}{\sqrt{1 + TDH_{fund}^2}} \cos \varphi_1 \quad [1.4]$$

where $\cos \varphi_1$ represents the *displacement factor*, in other words the phase shift between the current fundamental and the voltage.

We can therefore see that the presence of harmonics increases the apparent power of a certain appliance or piece of equipment. This influence can equally be rendered as a power balance showing the apparent power, active power, reactive power and deforming power (showing the harmonic distortion). This relation for a grid with q phases is of the form:

$$S^2 = P^2 + Q^2 + D^2 \quad [1.5]$$

with:

Simple voltage: V

RMS current per phase: I

Current fundamental: I_1

Apparent power: $S = q \ V \ I$

Active power: $P = q \ V \ I_1 \ \cos \varphi_1$

Reactive power: $Q = q \ V \ I_1 \ \sin \varphi_1$

Deforming power: $D = q \ V \ \sqrt{I_2^2 + I_3^2 + \dots} = q \ V \ I_1 \ \text{TDH}_{\text{fund}}$

Thus, the presence of harmonics degrades the quality of the electrical energy; it leads to additional losses, vibrations in rotating machines that contribute to the decrease in their longevity.

1.2.3. *Relevant standards for harmonic emissions*

The standard EN 61000-2-2 defines the levels of compatibility for low-voltage public networks and the standard 61000-2-4 defines them for medium- and high-voltage industrial applications. These levels are defined with regard to the network voltage deformations common to different kinds of equipment. We acknowledge that the number of harmonic sources will increase and that the proportion of purely resistive loads (electrical heating), which have a damping effect, will decrease relative to the total consumption. The levels of compatibility for individual harmonics in low-voltage grids are given in Table 1.1.

When several harmonics appear simultaneously, we can express their combined effect by the total harmonic distortion rate (THD_{fund}). Taking into account the levels given in Table 1.1 and that the individual harmonics do not simultaneously reach their level of compatibility, the compatibility level for the global harmonic distortion rate must be limited to 0.08.

Odd harmonics not including multiples of 3		Odd harmonics that are multiples of 3		Even harmonics	
Harmonic order (n)	Harmonic voltage (%)	Harmonic order (n)	Harmonic voltage (%)	Harmonic order (n)	Harmonic voltage (%)
5	6	3	5	2	2
7	5	9	1.5	4	1
11	3.5	15	0.3	6	0.5
13	3	21	0.2	8	0.5
17	2	>21	0.2	10	0.5
19	1.5			12	0.2
23	1.5			>12	0.2
25	1.5				
>25	$0.2 + 0.5 \times \frac{1}{25n}$				

Table 1.1. *Compatibility levels for individual harmonic voltages in low-voltage grids*

As we saw previously, the majority of low-frequency perturbations generated and endured by low-voltage equipment are linked to harmonic perturbations. These perturbations are therefore subject to international and European regulations. We will provide the content of the European regulations regarding the limitations of harmonic currents injected into the public power supply network (current used by appliances ≤ 16 A per phase). This standard is referred to as EN 61000-3-2.

1.2.4. Classification of appliances

Concerning the limitation of the harmonic voltage, appliances are classified in the following way:

Class A: balanced three-phase appliances and all other appliances with the exception of those that are labeled as being in one of the following classes.

Class B: portable tools (short-term use).

Class C: lighting appliances including light dimming devices.

Class D: appliances with an input current such that its wave shape at each normalized half-period relative to its peak value is within the range defined in Figure 1.5 (in fact at least 95% of the time) and with an input power of less than 600 W.

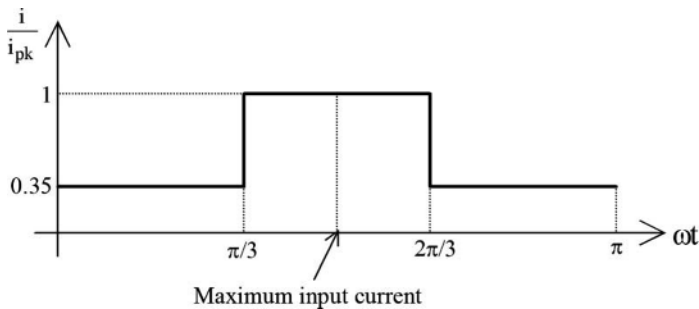


Figure 1.5. Shape of the current for class D of the EN 61000-3-2 standard

Regardless of the shape of the input wave, the appliances in class B and class C and motorized phase control appliances are not considered class D appliances.

1.2.5. The limits of harmonic currents

They are given in RMS.

Class A appliances: the input current harmonics must not exceed the values indicated in Table 1.2.

Class B appliances: the input current harmonics must not exceed the values indicated in Table 1.2, multiplied by a factor of 1.5.

Class C equipment: we must differentiate lighting appliances and light dimmers. The limits of harmonic currents in lighting appliances must not exceed the limits indicated in Table 1.2.

Harmonic order	Maximum authorized harmonic order (A)
Odd harmonics	
3	2.30
5	1.14
7	0.77
9	0.40
11	0.33
13	0.21
$15 \leq n \leq 39$	$0.15 \times 15/n$
Even harmonics	
2	1.08
4	0.43
6	0.30
$8 \leq n \leq 40$	$0.23 \times 8/n$

Table 1.2. Limits for class A appliances

For light dimmers that are either independent or incorporated into lamps, the following conditions must apply:

- For independent light dimmers, the values of the harmonic currents incorporated into incandescent lamps must not exceed the values in Table 1.2. When we use a phase-shift command, the firing angle must not exceed 145° .

- For discharge lamps in maximum charge conditions, the value of the harmonic current must not exceed the values defined in percentages in Table 1.2.

- For all positions of the light dimmer, the value of the harmonic currents must not exceed the limits defined in the case of a maximum charge.

Class D appliances: the limits of the harmonic currents are defined in the assigned load conditions. The input current harmonics must not exceed the limits in Table 1.4.

The limits given in Table 1.3 are valid for all appliances whose active input power is greater than 50 W. There are no limits for appliances with an active input power of less than 50 W.

Harmonic order	Maximum authorized harmonic current expressed as a percentage of the fundamental input current of the lighting (%)
Odd harmonics	
3	30 λ (λ : power factor of the circuit)
5	10
7	7
9	5
$11 \leq n \leq 39$	3
Even harmonics	
2	2

Table 1.3. Limits for class C appliances

Harmonic order	Maximum authorized harmonic current per watt (mA/W)	Maximum authorized harmonic current (A)
Odd harmonics		
3	3.4	2.30
5	1.9	1.14
7	1.0	0.77
9	0.5	0.40
11	0.35	0.33
$11 \leq n \leq 39$	$3.85/n$	$0.15 \times 15/n$

Table 1.4. Limits for class D appliances

1.2.6. Examples of observations of harmonic currents

Figure 1.6 shows the measurements² taken for several household appliances. We note that they have a high harmonic content. We also observe that the voltage waveform is clipped, so not perfectly sinusoidal, showing the consequences of current harmonics and of an insufficiently low impedance.

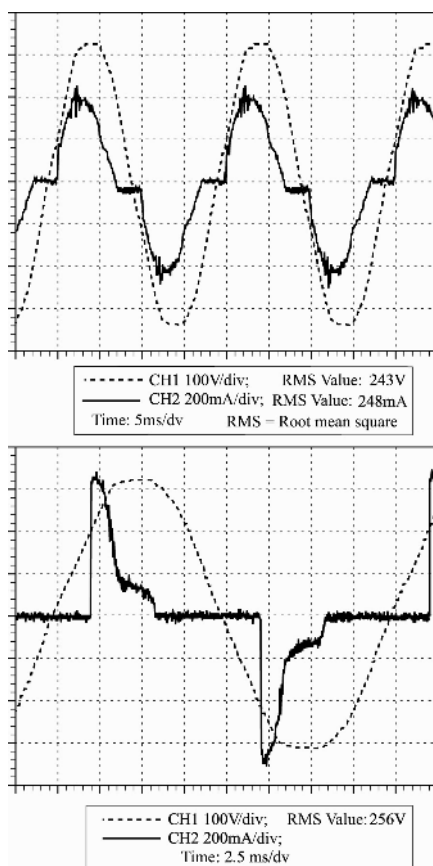


Figure 1.6. Examples of current and household appliance voltage waveforms measurements highlighting the harmonic content

² Measurements provided by J.P. Ferrieux, IUT of Grenoble.

These appliances are produced in very high quantities and therefore contribute to a heavy pollution of distribution networks. We can see especially that energy saving lighting does not represent progress from this point of view; certain office buildings in which the consumption is determined by fluorescent lighting and computing appliances (PC, monitors, printers, etc.) generate a very high level of odd harmonics that require specific reduction methods or the resizing of neutral conductors.

1.2.7. *Fluorescent lighting scenario*

The principle of operation of a fluorescent tube is described in Figure 1.7. The tube has two electrodes at each extremity, and is filled with an inert gas and a small quantity of mercury (in liquid form and in gas form before ignition). The interior of the tube is lined with a mixture of different fluorescent powders. These powders allow the conversion of ultraviolet radiation into several rays situated in visible frequencies. Numerous different powders exist, which can give practically all color temperatures (from hot to cold colors).

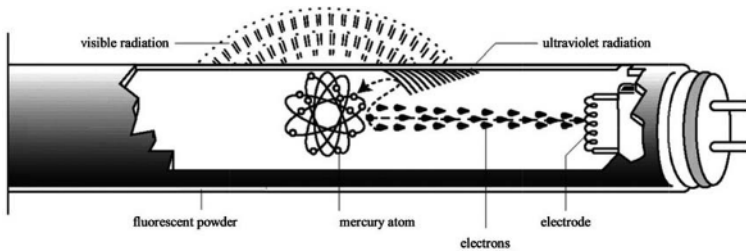


Figure 1.7. *Principle of light emission of a fluorescent tube*

Nevertheless, these lamps have excellent luminous outputs that cannot, as opposed to traditional incandescent lamps, be placed directly on the electrical network. Indeed, the electrodes of the majority of these tubes must be

preheated to facilitate ignition (vaporization of mercury). This means that a voltage dedicated to the preheating must be applied before executing the ignition. The ignition of the tube (ignition of the ionization process) is thus realized through the application of a high voltage at the ends of the two electrodes. Moreover, once it is ignited, its negative resistance (Figure 1.8) renders its direct connection to the network impossible. These lamps can therefore only work when combined with an electrical ballast (reactive impedance) allowing for control of the preheating and dimming, and for the limitation of the current circulating in the tube by ensuring stable operation. Indeed, we can observe that due to the distinctive negative resistance, any point of operation where constant voltage is imposed is unstable.

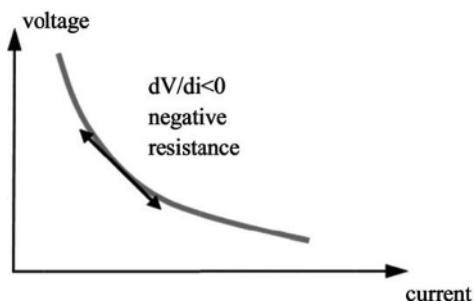


Figure 1.8. *Distinctive negative resistance of a fluorescent tube*

The simplest ballast consists of an iron core inductance operating in tandem with a “starter” for the ignition. The corresponding diagram is shown in Figure 1.9. The combination of the ballast and the lamp acts as a complex form of impedance, but presents a partly positive impedance. This provides a stable operating point in a fixed-voltage grid on the condition that it is placed beyond a voltage limit V_{\min} .

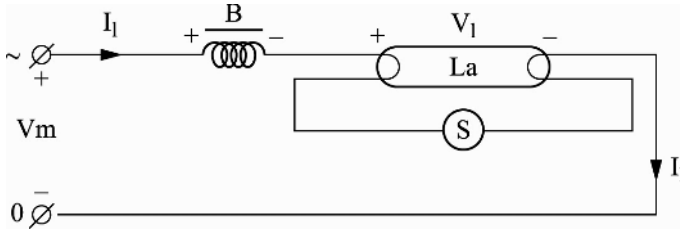


Figure 1.9. Power supply of the tube through an intermediate ballast

The curves shown in Figure 1.10 can be determined by only taking into account the fundamental components of the different quantities, particularly for the voltage at the terminals of the tube. The calculations enabling this construction are given below:

$$\begin{aligned}
 V_{ballast} &= jL\omega I_1 & V_{lamp} &= f(I_1) \\
 V &= V_{ballast} + V_{lamp}
 \end{aligned}
 \tag{1.6}$$

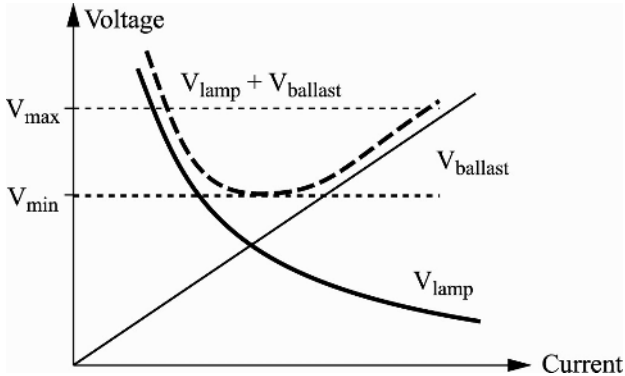


Figure 1.10. Electrical characteristic of ballast+lamp

Thus, the ballast can be resized in such a way that a correct operation of the lamp can be ensured in the possible variation range of the grid RMS voltage. Indeed, we must ensure that the minimum voltage is greater than V_{min} and that the maximum voltage V_{max} is compatible with the

maximum power that the lamp can consume. This power is in fact limited by the temperature maintained by the electrodes.

When the lamps are powered by the 230 V/50 Hz electric network through a magnetic ballast (as in Figure 1.9), the voltage at the terminals of the lamp and the current that travels through it are not sinusoidal (see Figure 1.11). Each time the current passes through zero, the lamp is neutralized and requires a certain voltage in order to be reignited. The lamp being “hot”, this voltage is much weaker than that required for the initial ignition. This re-ignition phase is shown as a slight overvoltage appearing at the start of each half-period. The power factor of the lamp will therefore not exceed 0.8 due to the high deformation of the two quantities.

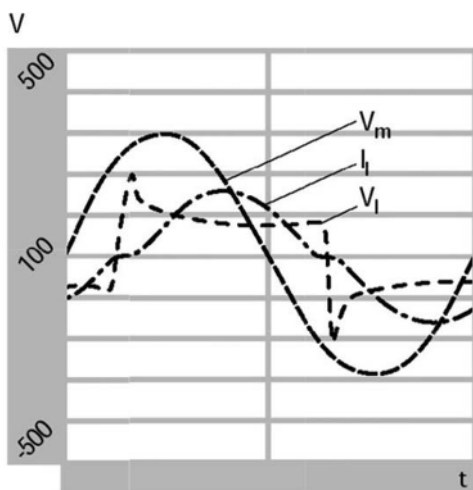


Figure 1.11. Evolution of the electrical quantities in the fluorescent lamp

As we can see from the shape of the current as shown in Figure 1.11, the current is not strictly sinusoidal. The deformation of the current is linked both to the square waveform of the voltage at the terminals of the lamp and

also to the nonlinearity of the inductance making up the ballast (hysteresis). Measurements performed on tubes in a stabilized state give the following typical values:

Harmonic order	Amplitude (%)	NF EN 61000-3-2
Fundamental	100	100%
3	10	30%
5	3	10%
7	2	7%
9	1	5%

Table 1.5. Typical values of current harmonic rates for a fluorescent lamp

Nevertheless, the power factor of the ballast/lamp combination is approximately 0.5. The total third-order harmonic distortion is thus limited to 15%. This equipment therefore conforms to the prescribed values.

1.2.8. Practical scenario of the improvement of the total harmonic distortion generated by a variable-frequency drive

Let us consider the following case of a variable-frequency drive using the variable-frequency control of a three-phase induction motor starting from the single-phase electrical network. The principle of this power supply is illustrated in Figure 1.12. The temporal curves of the current and its measured harmonics in this type of equipment with the help of a network analyzer are shown in Figure 1.13.

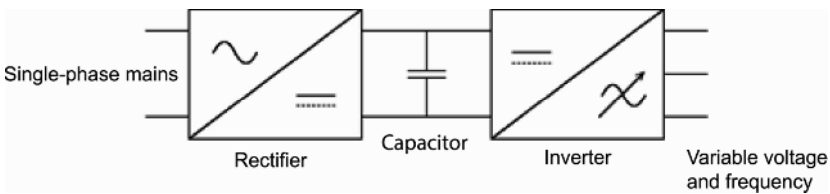


Figure 1.12. Structure of the variable-frequency drive

Since this equipment functions on the low-voltage mains and absorbs a current less than 16 A, we can refer to the NF EN 61000-3-2 standard in order to determine the permitted harmonic levels for it. The current absorbed by this equipment is such that it must be considered as a class D appliance. The limits for the permitted harmonic perturbations are given in Table 1.4. The values of these limits from the table can be calculated by using a nominal absorbed power of 750 W and a limit of 2.3 A for the third-order harmonic. It is obvious that in this configuration, the variable-frequency drive does not conform to the regulations. Indeed, if we were to only consider the third-order harmonic, we would obtain a value measured at 2.74 A. The variable-frequency drive therefore does not strictly conform to the regulations. Thus, it is necessary to reduce the harmonic currents.

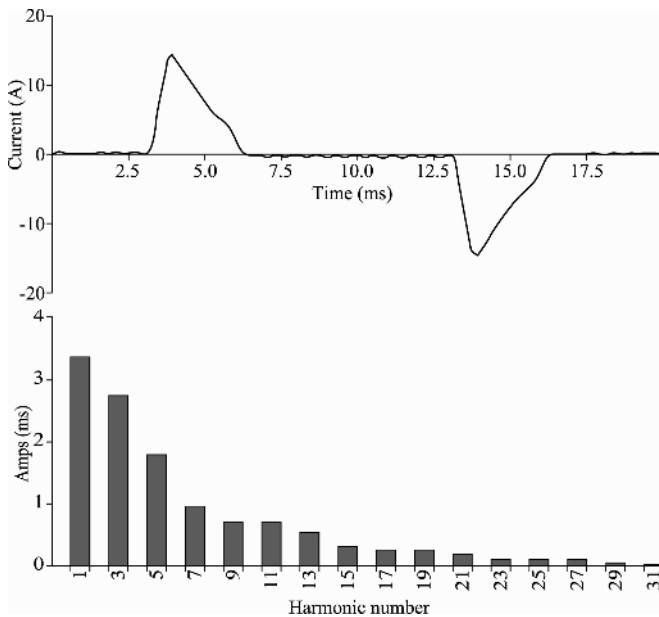


Figure 1.13. Current absorbed at the input of the variable-frequency drive as a function of time and representation of the harmonics

One possible solution consists of adding an inductance in series with the variable-frequency drive. The corresponding diagram is given in Figure 1.14.

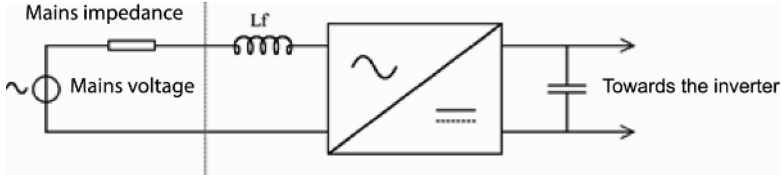


Figure 1.14. *Structure of the variable-frequency drive with an inductance in series*

The presence of an inductance in series helps to reduce the harmonic currents absorbed by the variable-frequency drive. Nevertheless, we note that its value is limited for two reasons: its presence damages the displacement factor of the system through the phase shift of the current fundamental in relation to the voltage. This inductance causes a voltage drop that results in a reduction of the voltage on the continuous bus. For these two reasons, the value of this inductance cannot exceed 10 mH in this example. The results from measurements and the wave shape of the absorbed current are given in Figure 1.15. We can verify that the equipment comprised of the variable-frequency drive/inductance combination now conforms to the EN 61000-3-2 standard.

The analytical calculation of this inductance is quite complex provided we take into account the different constraints we have mentioned (voltage drop, power factor). It is also preferable to resort to the computer simulation. This example has thus been modeled with the equivalent diagram in Figure 1.16 in order to precisely determine the value of L by paying particular attention to the impedance of the source. The values of the simulation components are indicated in the diagram, which help to find the observed electrical values, as shown in Figure 1.17.

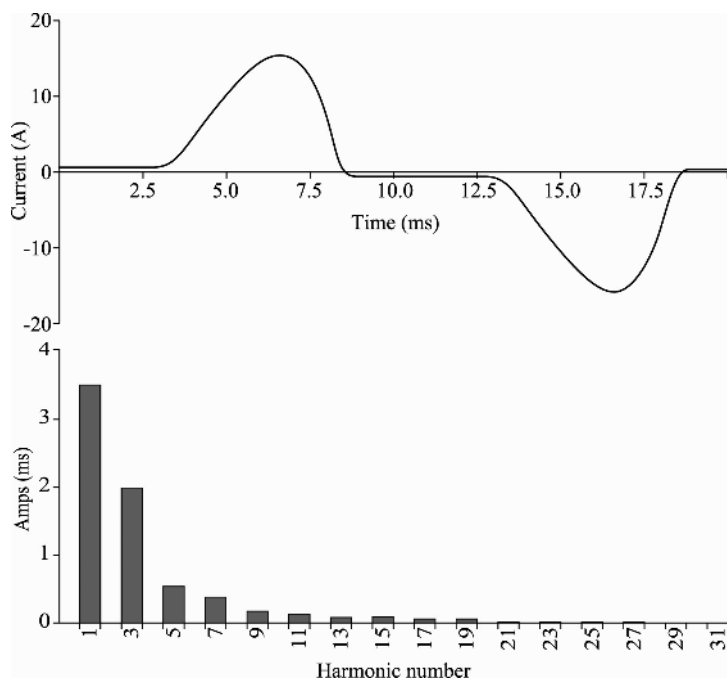


Figure 1.15. Current absorbed at the input of the variable-frequency drive as a function of time and representation of the harmonics

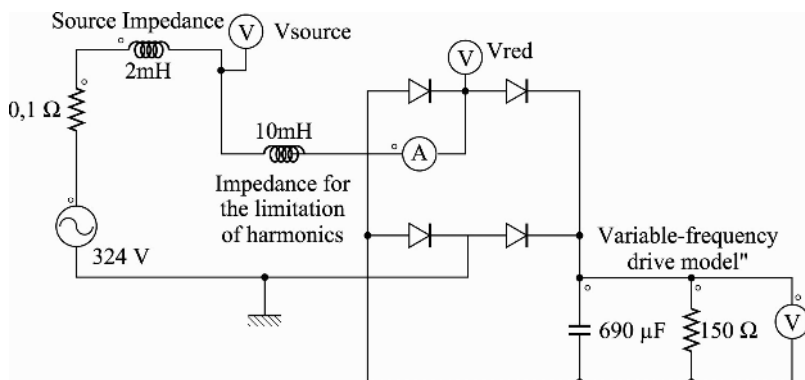


Figure 1.16. Diagram of the simulation used to determine L

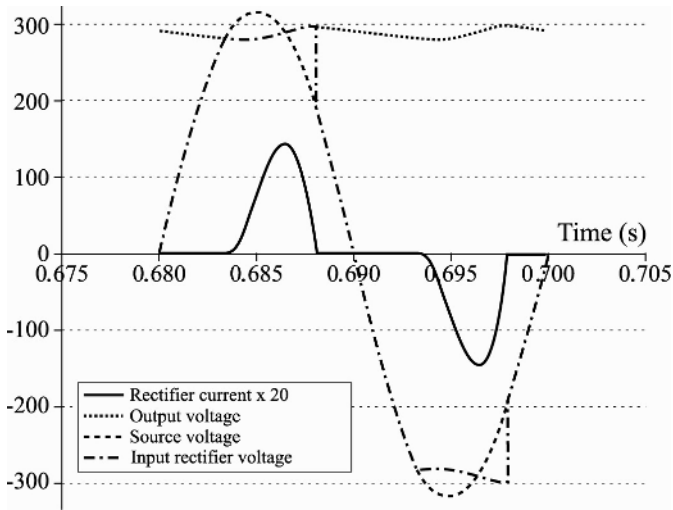


Figure 1.17. Simulated waveforms

1.2.9. Converter with sinusoidal absorption

The goal is to make sure that the equipment absorbs a current that is as close as possible to a sine curve.

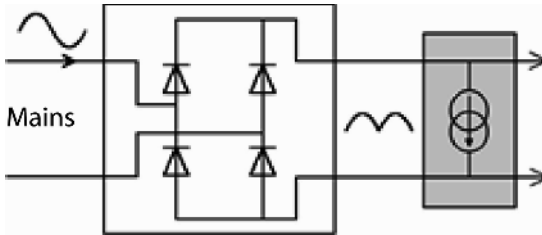


Figure 1.18. Principle of sinusoidal absorption of current of a converter

The current absorbed by the equipment, which is placed behind the diode bridge, must therefore be in the shape of a sine curve reflecting the rectified voltage network (see Figure 1.18). If the dynamic of the system is sufficient, the device will absorb a sinusoidal current in phase with the

electrical network at all times. The absorbed energy is stored in a capacitor, which itself, provides this energy to the load. The combination of diode bridge/power factor corrector (PFC) behaves, with regard to the mains, as a linear resistive load.

1.2.9.1. Principle of operation of a PFC

As we have seen, it involves the creation of a source of current in the shape of a sine curve. The immediate power quantities in play being large, these systems operate on the electrical principle of switching. The most commonly used structures in the field are structures that connect to sources of voltage. The interfacing of the source of voltage and the rectified mains is accomplished because of an inductance. The current control provided by the PFC is therefore executed through the intermediary of a control loop that helps to determine the waveform of the voltage to be generated at each instant. The previously outlined principle is illustrated in Figure 1.19.

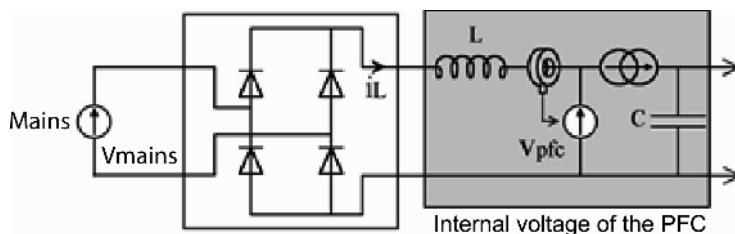


Figure 1.19. Principle of a power factor corrector (PFC)

The internal voltage can be calculated at each instant using the following method:

$$v_{PFC} = |v_{main}| - L \frac{di_L}{dt} \quad [1. 7]$$

The corresponding waveforms for different inductance values are given in Figure 1.20.

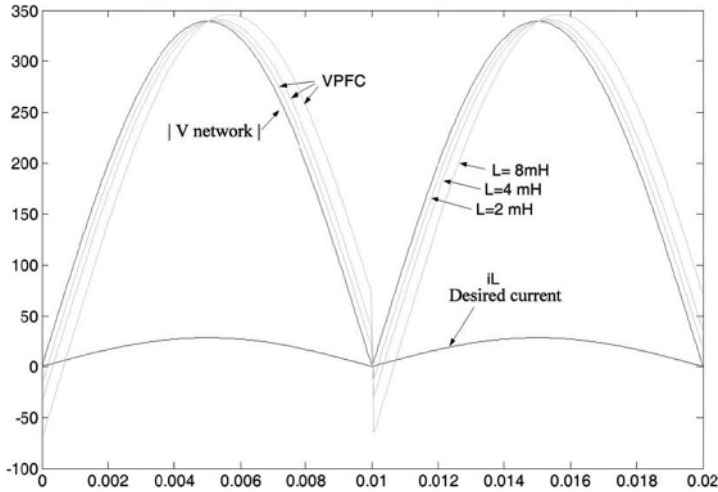


Figure 1.20. *Distinctive waveforms of a PFC*

The observation of these curves shows that the internal voltage of the PFC has a higher peak value than the maximal voltage of the mains. This voltage will incidentally be higher as the inductance has a higher value. We can equally note that the internal voltage of the PFC must become negative in order to obtain the desired current waveforms. A negative voltage can only be obtained through the use of a reversible voltage conversion system, although for reasons of cost, and since the duration for which the voltage is negative is relatively short, the choice consists of a unidirectional voltage structure. The internal voltage of the PFC can therefore not become negative. As a result, this limitation systematically produces a distortion in the waveform of the current as it approaches the crossing through zero.

The structure which enables the generation of the PFC's internal voltage must now be chosen. The immediate power circulating in the PFC is such that the choice of electronic switching is the only solution. The internal source is therefore produced through the intermediary of a chopper

via the switching of the voltage at the terminals of the tank capacitor. This corresponds to the diagram in Figure 1.21.

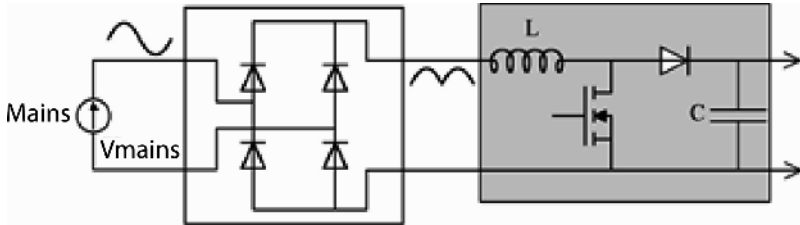


Figure 1.21. Structure of the BOOST-chopper-derived PFC

We can note that in these structures, the inductance plays two parts. It acts as a ballast between the rectified mains and the internal voltage of the PFC, as without it the internal voltage would need to be strictly equal to the network voltage and the current would not be able to be regulated. We acknowledge that this inductance also acts as a smoothing inductance for the chopper. Indeed, this system functions on the principle of switching and thus generates square waveforms in the modulated voltage (pulse-width modulation (PWM)). It is obviously not an option to insert high-frequency currents into the mains, which make the smoothing of the currents, as provided by the chopper, necessary. The choice of inductance therefore results in a compromise between the efficiency of the filtering and, as we saw previously, the voltage value at the terminals of the tank capacitor. The control of this system is therefore executed by regulating the current absorbed by the filter. The diagram of the principle behind this regulation is given in Figure 1.22.

We must now turn our attention to the choice of amplitude of the current to be injected into the control loop. We will analyze the system in terms of energy transfer. Supposing that the control loop functions perfectly, the DC-DC converter absorbs a current in the shape of sine curves,

the amplitude of which is given by I_{ref} . The power absorbed by the system is therefore entirely fixed. Indeed, this power is equal to:

$$P_{abs} = V I_{ref} / \sqrt{2} \quad [1.8]$$

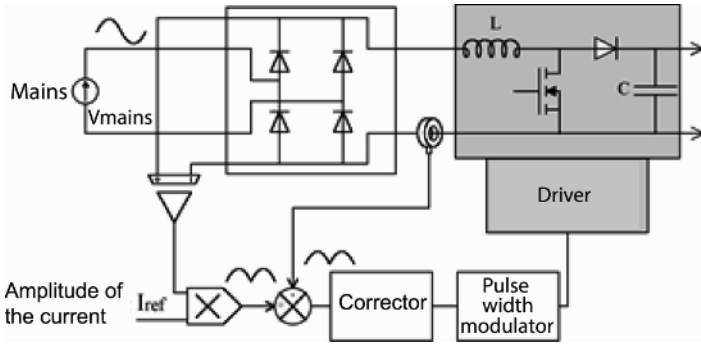


Figure 1.22. Diagram of current control in a PFC

The power consumed by the charge depends on the voltage at the terminals of the tank capacitor.

$$P_{load} = f(V_c)$$

Without control over the input power, these two values cannot be equal. Thus, if $P_{abs} > P_{load}$, the tank capacitor charges itself (the voltage increases). Alternatively, if $P_{abs} < P_{load}$, then the capacitor discharges itself. Therefore, there is no possibility of having stable operation without having control over the amplitude of the absorbed current. Determining the amplitude of the current to be absorbed can be done by using a control loop for the voltage at the terminals of the capacitor. This loop, which has the role of maintaining the capacitor's voltage close to a prescribed value, will modify the amplitude of the absorbed current in order to reach this target. Let us recall that this voltage must be greater than the maximum voltage of the mains,

without which the PFC loses control of the shape of the input current. The principle of this control method is shown in Figure 1.23.

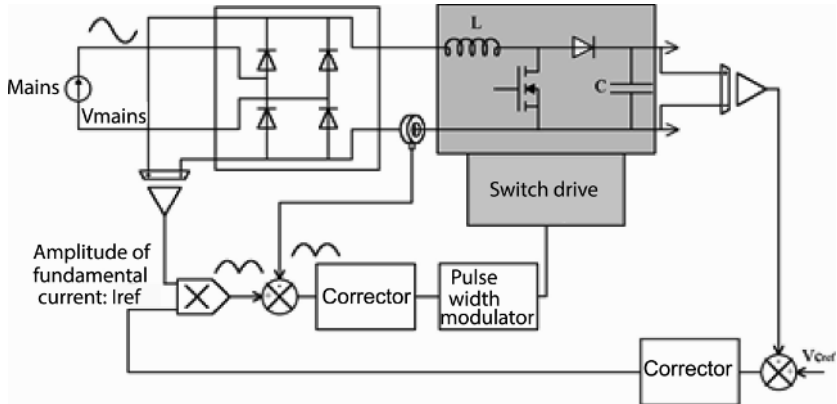


Figure 1.23. *Diagram of the control of the input current and output voltage of a PFC*

This example shows how to approach the problem of harmonic currents in the mains created by a static converter. The implemented solution is based on the use of a chopper which switches at a high frequency compared to the frequency of the electrical network. We will see in Chapter 2 that this principle also generates high-frequency perturbations; a case study will revisit this PFC structure and will analyze it from this aspect, completing this initial low frequency (LF) analysis.

1.3. Common-mode and differential-mode conducted perturbations

If the grid harmonics are in synchronization with the voltage wave of the mains and multiples of 50 Hz, those created by the power-electronic systems are multiples of the switching frequency of each device. Their method of

propagation is equally more complex. Indeed, their propagation can be executed on energy lines (like grid harmonics) and also via information transmission lines. Circuit breakers for HF parasite currents can use the earth or ground of appliances, made up of loops with very large surface-areas. The conductors used by high or very high frequency currents can then act as antennae and emit these parasite signals. Thus, it is necessary to separate the *conducted and radiated perturbations* and their different methods of propagation and/or their coupling with the environment [PAU 92].

For this, it is necessary to define a frame of reference and borders for the environment of the system through which they will propagate through conduction.

1.3.1. *Common mode and differential mode*

To study the methods of conducted propagation, it is practical to define a model of electrical links between “boxes” that constitute the borders of the subsystem or equipment in question. We must assign a fixed potential (ground plane, rack, earth) to each “box”, to which every subsystem is connected in a more or less local or direct manner. We note that the majority of electrical appliances are equipped with an earth plug; therefore, they are connected to a common reference which is the earth, and the impedance of these links depends on the quality of the earthing. An illustration is given in Figure 1.24 with the example of a switch-mode power supply which powers a load. We can define equivalent perturbation sources (voltage or current) that will allow, via the connection between the converter and the load, the circulation of parasite currents. They loop themselves by following the links in the same direction and by closing themselves through the earth or the common reference, which is the *common-mode* propagation, or in the inverse direction, which is *differential-mode* propagation.

The sources that created these currents are also called common-mode sources or differential-mode sources; in this example, we chose to represent two common-mode voltage sources and a differential-mode source of current. The nature of the source depends on the type of equipment. The parasite currents are determined in part by the impedances through which they are closed off; some are perfectly determined, which in this case would be “physical” differential-mode impedance of the load, while others are more diluted, in which case it would be common-mode impedances that often correspond not to real components but to undesirable coupling effects: capacitive, mutual, insulation faults, etc.

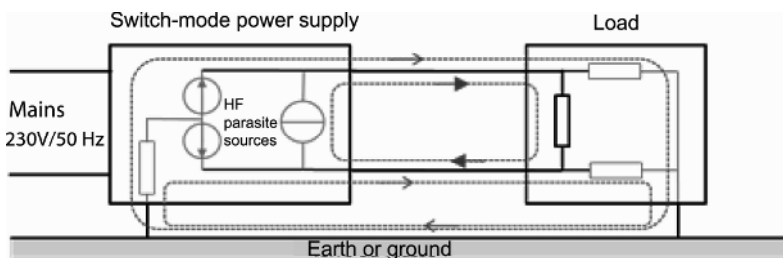


Figure 1.24. Sources and propagation methods: common mode and differential mode

This method of representation also allows us to model how perturbations are transmitted through an electrical system, which is known as the coupling method. In a conducted system, in addition to the direct coupling method that is illustrated in Figure 1.24, the main coupling method is said to be through “common impedance”.

Coupling through common impedance is possible when the source and the “victims” are connected to the same impedance, for example, devices in derivation on the same supply line or electronic functions routed through the same power supply bus. In differential mode, the perturbing current provokes voltage drops transmitted to the differential-mode “victims”, as shown in Figure 1.25. In

common mode, the parasite current generated by the source divides itself across the impedances of the source, the common lines and the “victims”, through the earth, also causing undesirable voltage drops. Their levels depend on the relative values of the impedances encountered. Thus, the parasite voltages that appear to be spread out over the common impedance are a result of the set of parasite sources.

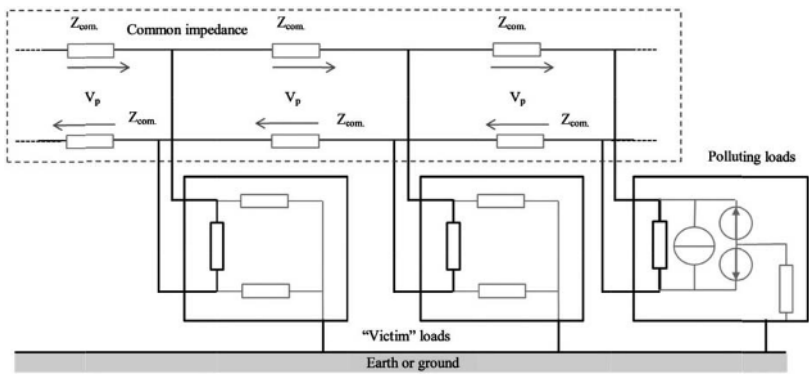


Figure 1.25. *Coupling through common impedance in common mode and differential mode*

In addition to the perturbations transmitted through galvanic contact, there are other methods of perturbation when an electromagnetic field interferes with conductors that connect devices, which is called “field-to-cable” coupling. The two components E and H of the parasitic field contribute to the induction in the cable of the parasite currents or voltages, in common mode and/or differential mode as represented in Figure 1.26. The H component in the field contributes to the appearance:

- of a voltage established by induction in common-mode V_{pMC} created by the magnetic flux traversing the area situated between the cable and the ground plane;

– of a voltage established by induction in differential-mode V_{pMD} due to a flux of H throughout the surface delimited by the two conductors of the link.

These voltages then create common- and differential-mode currents determined by the circuit in question. Generally, the surface of the common-mode loop is much larger than the surface of the differential-mode loop, which results in common mode being more sensitive to this perturbation.

The E component of the field in question contributes to the induction of common-mode currents I_{pMC} and differential-mode currents I_{pMD} .

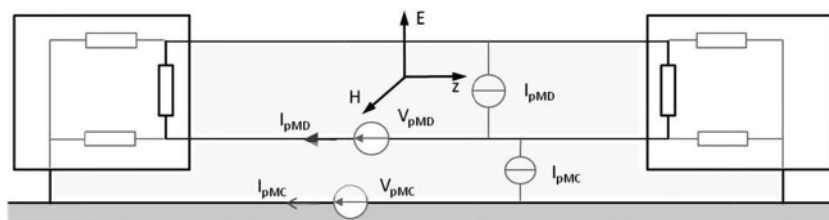


Figure 1.26. *Field-to-cable coupling in common mode and differential mode*

Example number 1: Disruption of measurements in a power-electronics environment.

A voltage probe of an oscilloscope is connected to a switch-mode power supply with an earth link (security of personnel) to carry out a measurement. The oscilloscope is itself earthed. Therefore, it constitutes a loop via the earth as shown in Figure 1.27. The transformer of the switch-mode power supply generates a flux in leaks and the amplitude of which depends on its power and technological make-up. The equivalent diagram represents the effects on the measurement:

– The leakage flux of the transformer establishes a voltage V_{mc} by induction through the loop made up of earth connections and the shielding of the wire:

$$V_{mc} = \int_{earth_loop} \mu_0 \frac{dH_p}{dt} ds \tag{1.9}$$

This voltage becomes larger as the frequency of H_p and the surface of the loop become larger.

– The voltage V_{mc} creates a current I_{mc} determined through the impedances of the loop: shielding of the probe, connection between earth and internal connection of the switch-mode power supply.

– The current is created by the parasite voltage V_p that is made up of the value V_0 measured by the probe.

– Finally, the input of the oscilloscope measures the voltage V_m tarnished by the error V_p :

$$V_m = V_0 + \frac{Z_{shielding}}{Z_{blindage} + Z_{earth} + Z_{wiring}} V_{mc} \tag{1.10}$$

Therefore, we note that the error in measurement depends on the various impedances of the loop and the effect from coupling of the parasite-leak field on the common-mode circuit.

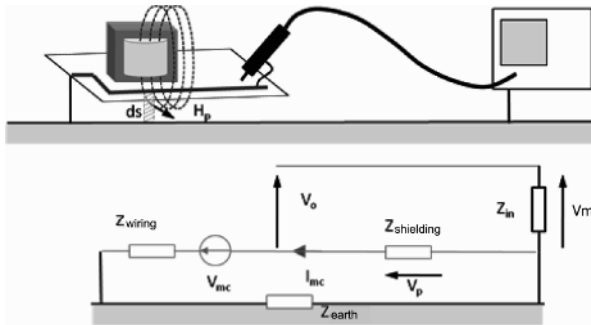


Figure 1.27. Example of H -field coupling during a measurement

Example number 2: Impact of a lightning bolt on a household appliance.

The lightning current, even if it does not strike the building directly can have severe consequences through its radiated and conducted effects. It is distinguished by a series of pulses in a current of various amplitudes, which travel through the ionized channel between the thunder cloud and the ground [UMA 87]. To simplify this analysis, we will suppose that the lightning current is represented by a rectilinear conductor traveled by one (or several) pulse(s) of bioexponential current(s) (see Figure 1.30) whose temporal features are shown in Figure 1.28(a) and defined herein:

$$I_{\text{lightning}} = I_0 \left(e^{-\frac{t}{\tau_d}} - e^{-\frac{t}{\tau_m}} \right) U(t) \quad [1.11]$$

$U(t)$ is the echelon function

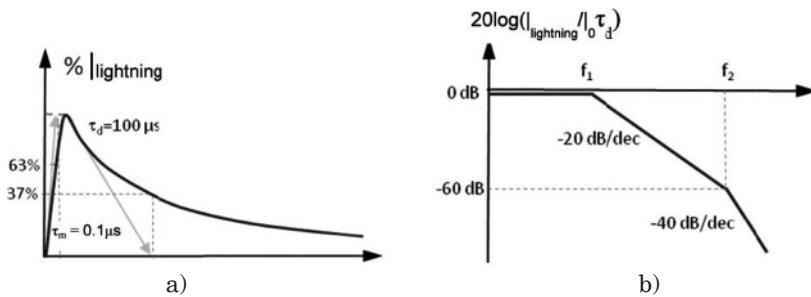


Figure 1.28. Characteristic a) time and b) frequency features of a lightning wave (specific teaching course)

The amplitude of the lightning current can reach 20–200 kA. The Fourier transformation given below helps to determine the frequency range of this wave; two distinguishable frequencies f_1 and f_2 appear that determine the frequency ranges over which the spectrum decreases to -20 dB/dec, then -40 dB/dec, as shown in Figure 1.28(b).

$$I_{lightning}(f) = \frac{I_0 \tau_d}{\sqrt{[1 + (2\pi\tau_m f)^2][1 + (2\pi\tau_d f)^2]}} \quad [1.12]$$

$$f_1 = \frac{1}{2\pi\tau_d} \approx 1.6 \text{ kHz} \quad f_2 = \frac{1}{2\pi\tau_m} \approx 1.6 \text{ MHz}$$

The lightning wave is therefore perturbing for frequencies less than a few megahertz. This representation in the frequency domain also helps to use the expressions of radiation of the antenna obtained in a sinusoidal system to calculate the field that was radiated by a lightning strike.

1.3.1.1. *Emitted effects*

The radiation formula of the Hertz dipole in spherical coordinates at a point P in space is given by the following expression below; we point out in Figure 1.29 the standard orientation of the angles as well as the parameters used.

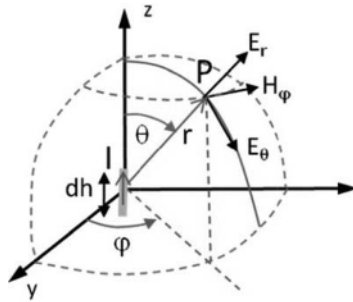


Figure 1.29. Standard orientation of the Hertz dipole

$$\begin{cases} E_r = \frac{Idh}{4\pi j\omega\epsilon_0} \frac{2\cos(\theta)}{r^3} (1 + j\gamma r) e^{-j\gamma r} \\ E_\theta = \frac{Idh}{4\pi j\omega\epsilon_0} \frac{\sin(\theta)}{r^3} (1 + j\gamma r + (j\gamma r)^2) e^{-j\gamma r} \\ H_\phi = \frac{Idh}{4\pi} \frac{\sin(\theta)}{r^2} (1 + j\gamma r) e^{-j\gamma r} \end{cases}$$

$$\text{with: } \lambda = \frac{c}{2\pi\omega}$$

$$\gamma = \frac{2\pi}{\lambda} = \omega\sqrt{\varepsilon_0\mu_0}$$

By simplifying these expressions in the case of a distant field³, specifically for $\gamma r \gg 1$, we obtain the following formulas:

$$E_r \approx 0$$

$$E_\theta \approx \sqrt{\frac{\mu_0}{\varepsilon_0}} j\omega\sqrt{\varepsilon_0\mu_0} \frac{I_0 dh \sin(\theta)}{4\pi r} \cdot e^{-j\gamma r} \quad [1.13]$$

$$H_\varphi \approx j\omega\sqrt{\varepsilon_0\mu_0} \frac{I_0 dh \sin(\theta)}{4\pi r} \cdot e^{-j\gamma r}$$

We represent this situation in Figure 1.30, where the lightning bolt (supposing it is vertical and traveled by a uniform current) of height h , situated at a distance d , radiates an electromagnetic field comparable to a plane wave at the observation point P, center of the loop S_b . We suppose the loop has small dimensions compared to h and d and is found in the field containing the lightning bolt. By using the theory of images in order to take into account the effects of the earth, the components H and E of the field are calculated by integrating the previous formulas over a height of $2h$ and by considering that the ratio h/d is such that the distance r remains virtually constant and equal to d :

$$r = \sqrt{d^2 + h^2} \approx d \left(1 + \frac{1}{2} \left(\frac{h}{d} \right)^2 \right) \approx d \quad \text{error} = 5\% \text{ if } h/d < 0,32$$

$$H_\varphi(\omega) = j\omega\sqrt{\varepsilon_0\mu_0} \frac{I(\omega) \text{arctg}\left(\frac{h}{d}\right)}{2\pi} \cdot e^{-j\gamma d} \quad [1.14]$$

$$E_\theta(\omega) = \sqrt{\frac{\mu_0}{\varepsilon_0}} H_\varphi$$

³ This hypothesis also signifies that the distance r is large compared to the wavelength, which implies that we consider the frequency components of the current to be sufficiently large: for the numeric examples chosen, they are greater than 100 kHz.

Hence, the following are the time domain formulas:

$$H_{\varphi}(t) = \sqrt{\varepsilon_0 \mu_0} \frac{dI(t - d\sqrt{\varepsilon_0 \mu_0})}{dt} \operatorname{arctg}\left(\frac{h}{d}\right) \quad [1.15]$$

$$E_{\theta}(t) = \sqrt{\frac{\mu_0}{\varepsilon_0}} H_{\varphi}(t - d\sqrt{\varepsilon_0 \mu_0})$$

The term $j\omega$ in the frequency formulas of the H and E fields corresponds to a derivation over time and the term $e^{-j\omega d}$ corresponds to a delay.

The surface S_b can be made up for example of the loop in the earth conductor of a modem in a home, the shielding of an Ethernet cable of length L_0 situated at a height h_c above the ground and the earth conductor of the computer. The formulas for the resulting current and voltage are given by [UMA 87]:

$$I_{pMC} = C_b h_c \frac{dE}{dt} = C_b \mu_0 h_c \frac{d^2 I_{lightning}}{dt^2} \operatorname{arctg}\left(\frac{h}{d}\right) \quad [1.16]$$

$$V_{pMC} = \mu_0 S_b \frac{dH}{dt} = \mu_0 S_b \sqrt{\varepsilon_0 \mu_0} \frac{d^2 I_{lightning}}{dt^2} \operatorname{arctg}\left(\frac{h}{d}\right)$$

C_b represents the parasite capacitance between the shielding of the Ethernet cable and the earth, the expression of which is given by:

$$C_b = \frac{2\pi\varepsilon_0}{\log\left(\frac{4h_c}{a}\right)} L_0 \quad [1.17]$$

where L_0 is the length of the cable, and h_c is its height relative to the ground and its diameter.

Therefore, we note that the second derivative of the lightning current determines these values.

1.3.1.2. Numerical application

The lightning current is of the biexponential type, its peak value being 20 kA, $\tau_m = 1 \mu\text{s}$, $\tau_d = 50 \mu\text{s}$. The expression of the maximum value of the derivative is given by:

$$\left(\frac{d^2 I_{\text{lightning}}}{dt^2} \right)_{\text{max}} \simeq - \frac{I_0}{\tau_m^2} \quad [1.18]$$

The data given for the perturbed circuit consists of: $L_0 = 5 \text{ m}$, $h_c = 1 \text{ m}$, $S_b = 5 \text{ m}^2$, $C_b = 41.5 \text{ pF}$, $d = 5 \text{ km}$, $h = 1.5 \text{ km}$.

We can deduce that the maximum values are $V_{\text{pMC}} = 19.4 \text{ V}$ and $I_{\text{pMC}} = 48.4 \text{ mA}$. The waveforms are exponential pulses. These values and their rapid variations are sufficiently significant to excite the normal mode of the line and thus to create common-mode currents in that loop that are susceptible to perturbing the digital connection or even cause irreversible damage to the electronic components.

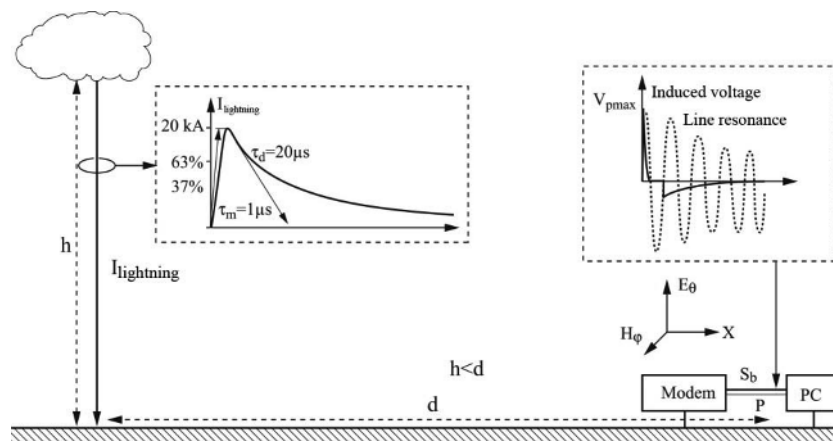


Figure 1.30. Effects radiated by a lightning strike on a circuit

1.3.1.3. Conducted effects

The ground has a resistance ρ which depends on its nature and humidity rate; therefore, a lightning strike will create a voltage wave $V(r)$ that will develop itself radially from the impact point according to the following law:

$$V(r) = \frac{\rho I}{2\pi r} \quad [1.19]$$

The lines of potential are spread along semi-hemispherical curves as shown in Figure 1.31.

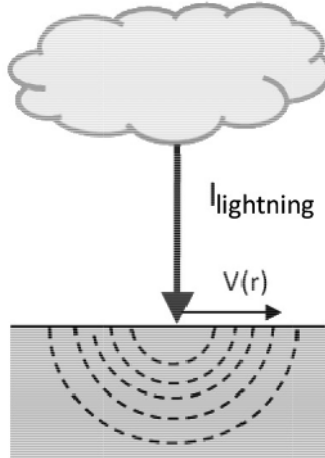


Figure 1.31. Voltage resulting from a lightning strike on the ground

Thus, an electric potential is developed between two earthed points and determined by the distance between these two points, the resistance of the ground and the intensity of the lightning. This voltage is responsible for the shocking of animals in fields or the destruction of electrical equipment in buildings where there are multiple distant earth connections.

1.3.2. Crosstalk

Crosstalk, sometimes referred to as “cable to cable coupling”, shown in Figure 1.32 is mentioned when connections are close together and perturb each other through capacitive coupling (C_{12}) and/or through mutual inductance (L_{12}). These couplings are distributed all along conductors 1 and 2, but if the length L_0 is small compared to the wavelength of the perturbing voltage V_0 , we can establish the equivalent lumped-elements circuit as shown in Figure 1.32.

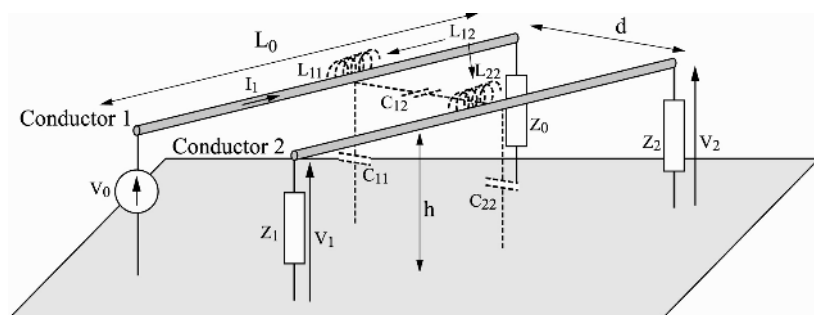


Figure 1.32. *Crosstalk between two conductors*

In this hypothesis, the source of perturbations V_0 injects a capacitive current via C_{12} and an inductive current resulting from mutual inductance L_{12} into the victim circuit comprised of conductor 2 and the impedances Z_1 and Z_2 . In Figure 1.33, we represent an electric model of crosstalk coupling where the effects are distributed symmetrically with regard to the middle of the opposite conductors; we suppose that the conductors have a low impedance compared to those of the end loads, which is generally the case. We can see that the effect from the crosstalk is different at the start and at the end of the target connection: the capacitive and inductive parasitic currents add to each other in one case and cut themselves off in the other.

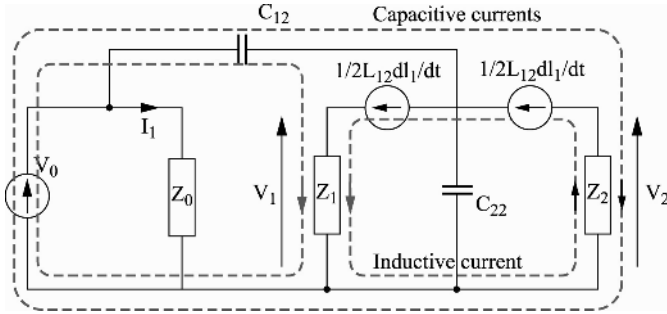


Figure 1.33. Electrical diagram of crosstalk coupling between two conductors

The expressions for the parasitic voltages V_1 and V_2 induced at the ends of the target connection are given by:

$$\begin{aligned}
 V_1 &= V_0 \left(p \frac{L_{12}}{2Z_0} + \frac{pC_{12} + p \frac{L_{12}}{2Z_0} \left(\frac{Z_1 - Z_2}{Z_1 Z_2} \right)}{p(C_{12} + C_{22}) + \frac{Z_1 + Z_2}{Z_1 Z_2}} \right) \\
 V_2 &= V_0 \left(-p \frac{L_{12}}{2Z_0} + \frac{pC_{12} + p \frac{L_{12}}{2Z_0} \left(\frac{Z_1 - Z_2}{Z_1 Z_2} \right)}{p(C_{12} + C_{22}) + \frac{Z_1 + Z_2}{Z_1 Z_2}} \right)
 \end{aligned}
 \tag{1.20}$$

Example number 3: When the diameter of the conductors is small compared to h and d , the linear expressions l_{ij} in the case of cylindrical conductors of diameter ϕ in the air above a ground plane are given by [GUE 02]:

$$l_{ii} = \frac{\mu_0}{2\pi} \ln\left(\frac{4h}{\phi}\right) \quad l_{ij} = \frac{\mu_0}{4\pi} \ln\left(1 + \frac{4h^2}{d^2}\right) \quad \text{for } i \neq j \tag{1.21}$$

The terms c_{ii} and c_{ij} are obtained through inversion of the matrix $[l_{ij}]$ given by:

$$[c_{ij}] = \epsilon_0 \mu_0 [l_{ij}]^{-1} \tag{1.22}$$

and finally the expressions corresponding to the length L_0 :

$$\begin{bmatrix} L_{ij} \end{bmatrix} = L_0 \begin{bmatrix} l_{ij} \end{bmatrix} \quad \begin{bmatrix} C_{ij} \end{bmatrix} = L_0 \begin{bmatrix} c_{ij} \end{bmatrix} \quad [1.23]$$

If we suppose that the impedances are identical at the ends of the target connection and that all impedances are resistances, the previous expression is simplified to:

$$\begin{aligned} V_1 &= V_0 \left(p \frac{L_{12}}{2R_0} + \frac{p \frac{R}{2} C_{12}}{1 + p \frac{R}{2} (C_{12} + C_{22})} \right) \\ V_2 &= V_0 \left(-p \frac{L_{12}}{2R_0} + \frac{p \frac{R}{2} C_{12}}{1 + p \frac{R}{2} (C_{12} + C_{22})} \right) \end{aligned} \quad [1.24]$$

Numerical application:

$L_0 = 10$ cm, $h = 10$ mm, $d = 10$ mm, $\phi_1 = 3$ mm, $\phi_2 = 1$ mm, the source of the disruption is a triangular alternative voltage generator with an amplitude of 25 V and a frequency of 500 kHz, $R_0 = 5 \Omega$, $R_1 = R_2 = 50$ k Ω .

We deduce that: $L_{11} = 52$ nH, $L_{22} = 74$ nH, $L_{12} = 32$ nH, $C_{11} = 3$ pF, $C_{22} = 2$ pF, $C_{12} = 1.5$ pF.

Figure 1.34 shows a simulation of this crosstalk, where we can clearly see that the voltages at the two ends are in the region of 2 V and different to each other. In these simple hypothetical cases, coupling is essentially due to derived effects; it is therefore increasing with the frequency.

According to the configuration of the influencing conductors and their shape, the amplitude of the currents and the voltage in the source conductor, one coupling mode can be dominant (magnetic or electrostatic); this hypothetical case therefore consists of ignoring either C_{12} or L_{12} in the model.

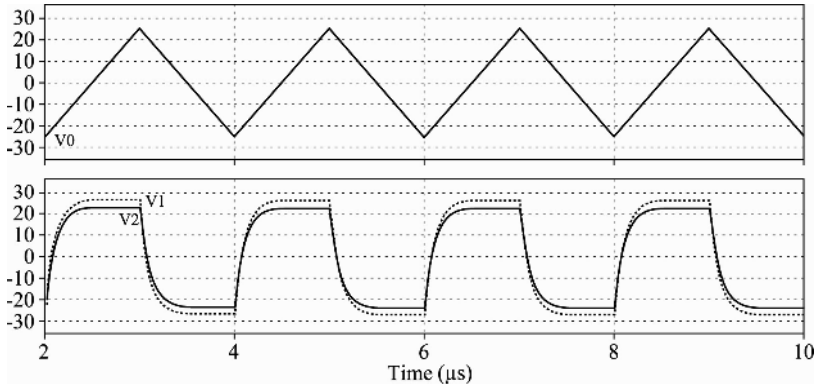


Figure 1.34. *Simulation of crosstalk coupling between two conductors*

1.4. Measuring electromagnetic perturbations

We distinguish two categories of measuring tools used in EMC. The first category involves the measuring of perturbations conducted at high frequencies; this includes the line impedance stabilization network (LISN) and the passive current sensors based on the principle of the current transformer. In the second category, we can find various types of antennae used to measure in the near or distant field. In every case, the signal from the sensor is analyzed in the time domain (oscilloscope) and more frequently in the frequency domain using the heterodyne spectrum analyzer.

1.4.1. *The line impedance stabilization network*

The LISN is connected to a filter fitted between the device being tested and the network supplying the energy. It has a dual purpose. In a standardized frequency range (150 kHz–30 MHz), it must isolate the network, in which common-mode and differential-mode perturbations may exist, from the equipment being tested. Nonetheless, it must provide an input-to-output voltage drop less than 5% of the nominal voltage to the frequency of the network when it is traveled

by the nominal current. Finally, it must present a terminating impedance that is constant with regard to the high-frequency perturbations emitted by the test device, in both common and differential modes, independent of the impedance introduced by the energy network. This impedance is standardized by CISPR (*Comité international spécial des perturbations radioélectriques* – Special international committee on radio interference) [INT 03a]. Figure 1.35 defines the limits in variation of this impedance, measured between an output terminal and the earth in the frequency range of 10 kHz–100 MHz. This range is divided into three bands (A, B, C). The corresponding diagram relative to each band is shown in Figure 1.35. The structure of the LISN is represented in Figure 1.36.

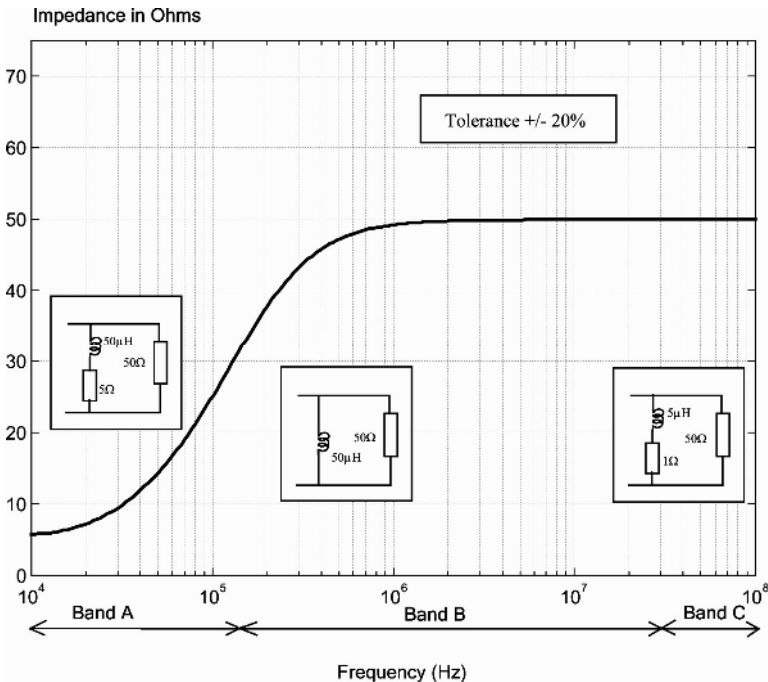


Figure 1.35. Common-mode impedance of the LISN

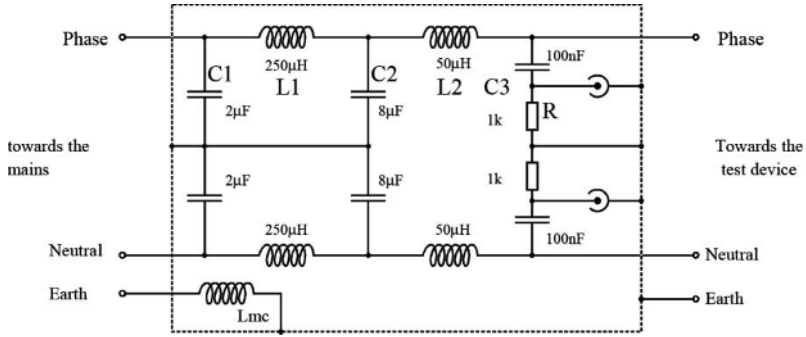


Figure 1.36. *Diagram of the principle of a single-phase LISN (according to document of Chase Electronics)*

The filter made up of L1, C1 and L2, and C2 is a low-pass filter that eliminates perturbations coming from the mains. The filter C3, R is a high-pass filter that enables the termination of high-frequency perturbations in the resistance R_0 of 50 Ω . The LISN can be used for currents with intensities up to 100 A. Past that, and for band A, it is possible to use a current probe.

1.4.2. Current sensors

The current sensors used in metrology in static conversion devices must have a very large bandwidth, in the hundreds of megahertz, must be capable of measuring high currents (up to several kiloamperes) and be insensitive to electromagnetic strikes released by the converter being tested. They are also used for measuring conducted parasitic currents. In this case, they must have a large bandwidth and not be prone to perturbations. Experience shows that passive sensors, based on the principle of the current transformer, are best suited to these metrological constraints, since knowledge of the DC component is not essential. The lumped-element electric model of such a device is shown in Figure 1.37.

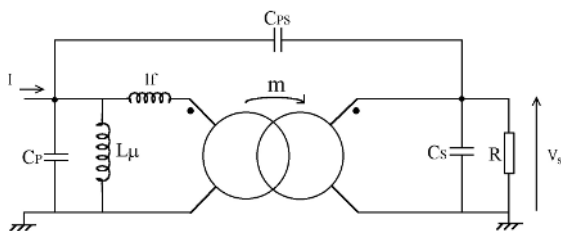


Figure 1.37. Model of the current transformer

This model allows us to understand the performance and limitations of this device. They involve the low cutoff frequency F_L , the linearity outside saturation, high-frequency operation and the resistance to electromagnetic perturbations.

1.4.2.1. Behavior at low frequency and the effects of saturation

At low frequency, the current transformer has a high-pass behavior. Its voltage transfer function V_s/I and its low cutoff frequency are given by the following expressions:

$$\frac{V_s}{I} = \frac{R}{m} \frac{j \frac{m^2 L_\mu}{R} \omega}{1 + j \frac{m^2}{R} (L_\mu + lf) \omega} \quad [1.25]$$

$$F_L = \frac{1}{2\pi} \frac{R/m^2}{L_\mu} = \frac{k}{2\pi \mu_0 \mu_r n \frac{A_e}{l_e}} \quad [1.26]$$

where A_e is the section of the magnetic circuit, l_e is the effective length of the magnetic circuit, n is the number of secondary turns, m is the transformation ratio (generally, there is one primary turn, hence $m = n$) and $k = R/n$.

These expressions are valid for a low-frequency band (<a few tens of kilohertz) in which the electrostatic effects

are negligible. The gain of this transfer function is given in Figure 1.38 (BF zone of the curve).

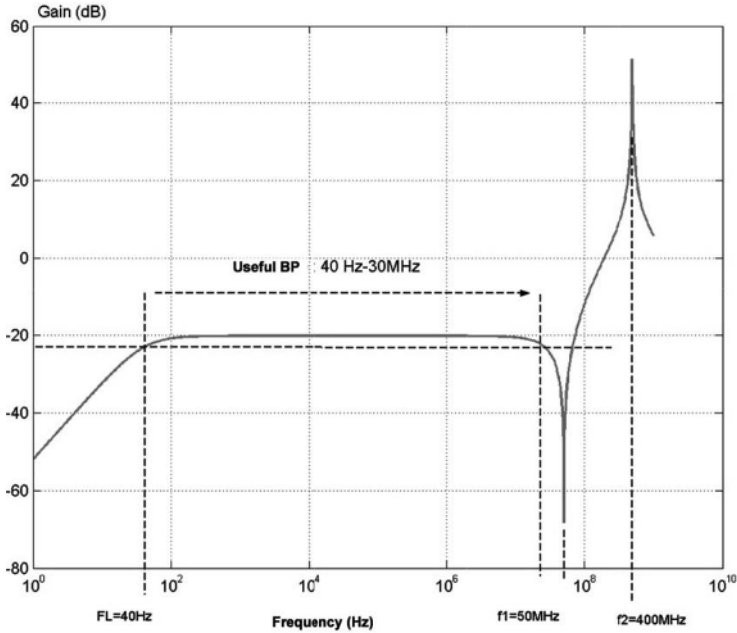


Figure 1.38. *Transfer function of the current transformer obtained through the model*

When the measured current has a DC or low-frequency component (outside its bandwidth), the magnetic circuit can be saturated, which translates into a distortion of the output signal. The expression below defines, in a sinusoidal system with a DC component, the limits in the linear operation of the device as a function of the quantities involved (DC current I_{DC} , maximum AC current I_{ACmax} , frequency ω and the specifications of the magnetic circuit: B_M , μ_r , specific inductance A_L , magnetic length l_e).

$$I_{ACmax} = \left(\frac{B_M}{\mu_0 \mu_r} l_e - I_{DC} \right) \sqrt{1 + \frac{(n^2 A_L \omega)^2}{R}} \tag{1.27}$$

In pulsed current, the saturation of the magnetic circuit is characterized by the maximum of the product $I \cdot T$. Its expression is given by:

$$(I \cdot T)_{\max} = \frac{n^2}{R} \cdot B_M \cdot A_e \quad [1.28]$$

1.4.2.2. Behavior at high frequency and with regard to perturbations

A third limitation appears for high-frequency operation. The expressions [1.26] and [1.27] show that to reduce F_L and increase $I_{AC\max}$, we must increase the number of winding turns n and the section of the magnetic circuit A_e . However, this is contradictory considering the high-frequency performances of the sensor. Indeed, the length of the secondary winding increases, just like the electrostatic phenomena (capacitances of the primary and secondary windings C_p , C_s), which limits the high-pass band of the sensor, as the current transfer function shows (see the HF section of the curve in Figure 1.38):

$$\frac{V_s}{I} = \frac{1 + l_f \cdot C_2 \cdot (j\omega)^2}{\frac{m}{R} + j\omega \frac{C_1 + C_3}{m} + (j\omega)^2 l_f \frac{m}{R} (C_1 + C_2) + (j\omega)^3 l_f \left(\frac{C_1 C_2 + C_1 C_3 + C_2 C_3}{m} \right)} \quad [1.29]$$

The capacitances C_1 , C_2 and C_3 are expressed as:

$$C_1 = C_p + C_{ps} (1 - m) \quad [1.30]$$

$$C_2 = m \cdot C_{ps} \quad [1.31]$$

$$C_3 = m^2 C_s + m(m - 1) C_{ps} \quad [1.32]$$

Two frequencies f_1 and f_2 are highlighted:

$$f_1 = \frac{1}{2\pi \cdot \sqrt{l_f \cdot m \cdot (C_p + C_{ps})}} \quad [1.33]$$

$$f_2 = \frac{1}{2\pi \cdot \sqrt[3]{\frac{l_f}{m} \cdot (C_1 \cdot C_2 + C_1 \cdot C_3 + C_2 \cdot C_3)}} \quad [1.34]$$

Calculating the transfer function was accomplished with typical values measured on a current transformer: $C_p = 0.1$ pF, $C_s = 100$ pF, $C_{ps} = 1$ pF, $m = 100$, $R = 10$ Ω , $l_f = 50$ nH.

For this example, the useful bandwidth at -3 dB stretches from 40 to 30 Hz. Beyond that, the parasitic effects begin to dominate: the series resonance lies essentially between the primary–secondary capacitance C_{ps} and the leakage inductance l_f (frequency f_1); then, for $f_1 < f < f_2$, we observe the dominant effect of the parasitic primary–secondary capacitance C_{ps} up until the parallel resonance frequency f_2 . Beyond the frequency f_1 , the current transformer is no longer usable.

Thus, the effects of primary-secondary capacitive coupling (capacitance C_{ps}) constitute a major limitation at high frequency, with the sensor acting as a high-pass filter. The result is the possibility of circulation of a common-mode current, prejudicial to measurements, as shown in Figure 1.39. Shielding between the primary and secondary of the device can limit these effects, with the parasitic capacitances C_{p1} and C_{p2} being in series. Finally, the cable connecting the sensor and the measuring tool can be influenced by high-frequency disruptive fields and by common-mode currents, which also translates into the deterioration of the measurement. To minimize these problems, it is preferable to insert the sensor into a conductor with low variability in order to limit the circulation of common-mode currents and

to reduce the impedance from the shielding as much as possible.

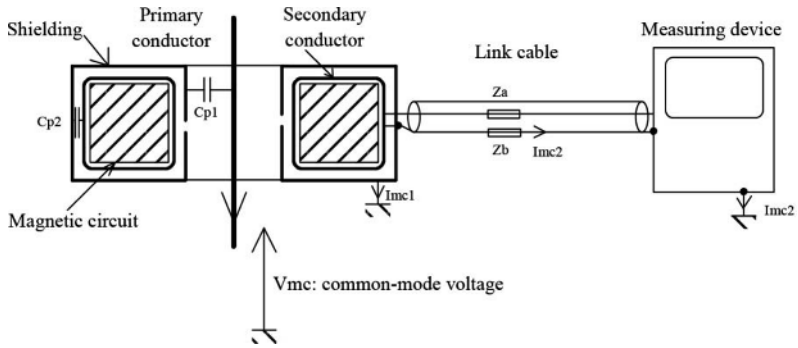


Figure 1.39. Reduction of perturbations to the sensor through protective coating

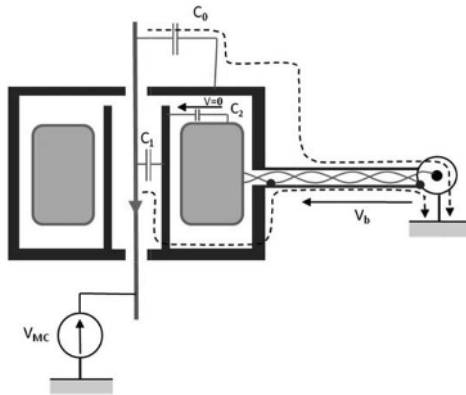


Figure 1.40. Sectional view of a current transformer with double shielding

In the case where we want a very strong immunity to common-mode currents, the alternative would be to use a shielded casing connected to a triaxial cable, as shown in the sectional view of the device in Figure 1.40. The parasitic common-mode currents resulting from either the conductor

having a variable potential V_{MC} or any other source of parasitic electrical fields in the environment are transported via C_0 through the shielded case and the shielding of the triaxial cable, and likewise for the one due to part of the conductor being inside the casing via C_1 . With the extremity of the secondary winding being connected to the shielded case, the current travelling through C_2 is non-existent. Thus, no common-mode current can circulate through the internal conductors of the cable that can perturb the secondary voltage of the transformer.

1.4.2.3. Available passive current sensors and their specifications

The sensors that currently exist on the market are limited to a frequency range of 4 or 5 decades, either toward the low frequencies (10 Hz–1 MHz) or toward the high frequencies (10 Hz–1 GHz). The curve in Figure 1.41 outlines the evolution of the high cutoff frequency with the current load, observed on existing products.

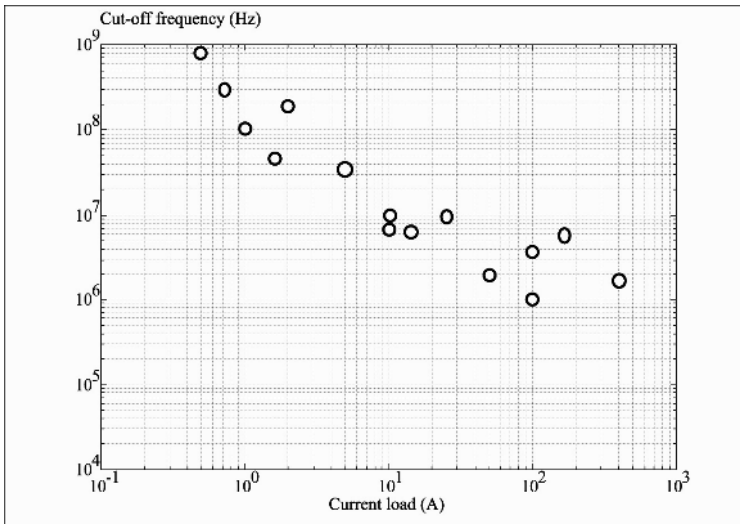


Figure 1.41. High cutoff frequency of current transformers as a function of the current load (according to doc. Pearson)

The specifications to take into account for choosing a sensor are therefore:

- the maximum current at different frequencies, generally at 50 Hz and the maximum usage frequency;
- the –3-dB bandwidth;
- the product $(I.T)_{\max}$ that outlines the saturation during the application of a pulsed current;
- the maximum DC component before saturation;
- the value of the load resistance;
- the insertion impedance;
- the geometric and physical data (diameter of the aperture, bulk, weight, etc.).

1.4.3. Antennae [KIN 82, BAL 97]

Antennae are used for close-field (in other words for a distance $d < \frac{\lambda}{2\pi}$) or far-field measurements ($d > \frac{\lambda}{2\pi}$, λ is the wavelength of the perturbing signal). In this last case, we consider plane-waves. The wave impedance, defined by the ratio $\frac{E}{H}$, is constant and measures 377 Ω in far-field.

Therefore, we only need to measure one of the two components in the electromagnetic field. The antennae for the far-field measurements are characterized by the following:

- The radiation pattern: this is the measurement of the amplitude E of the field emitted as a function of two angles defining the spherical coordinates of the space.
- The gain G , which is defined relative to an isotropic antenna emitting the same power:

G = maximum power density radiated in a specific direction/maximum power density uniformly radiated in every direction in space.

The gain of an antenna varies with the frequency; knowledge of this characteristic must be established for the frequency range.

– The antenna factor F_a : it is the relation between the field E and the voltage U measured at the ends of the antenna, which also varies with the frequency. It is established at a specifically predefined distance and is generally expressed in dB:

$$F_a = 20 \log\left(\frac{E}{H}\right)$$

The characteristics of antennae are adapted to the frequency range and the characteristics of the field that we want to measure. These characteristics must be as constant as possible in the frequency band being used. The references [INT 03a, INT 03b] define the characteristics of the antennae used in the measuring of fields. We will cite several currently used models.

– Band A (10–150 kHz), field H: observations show that it is the magnetic field that is responsible for the perturbations. The antenna is a loop in an electrically shielded frame and must fit within a square of 0.6 m.

– Band B (150 kHz–30 MHz), field H: we use the same device as in band A; field E: we use a vertical 1 m whip antenna for measuring a distance $d < 10$ m.

– Band C (30–300 MHz), field E: we use a balanced doublet antenna of length $\frac{\lambda}{2}$ for $F > 80$ MHz (λ corresponding to $F = 80$ MHz that being 3.75 m). Its symmetry is such that the measured level varies by at least

20 dB when its orientation passes from the parallel polarization direction to the transverse polarization direction. It is possible to use short doublet antennae (however their length is limited to $\frac{\lambda}{10}$), averaging the knowledge of their antenna factor. They are less sensible however. A frequently used model is the biconical antenna (Figure 1.42) that aims to present a large frequency range.

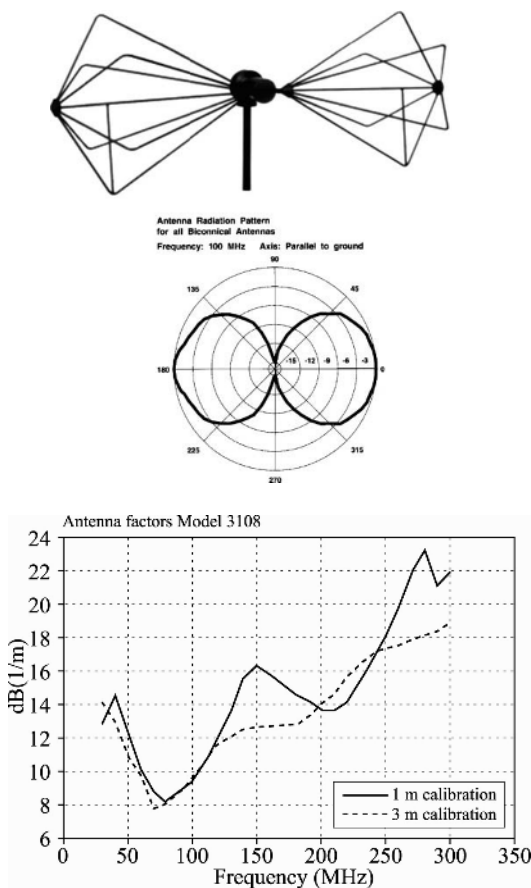
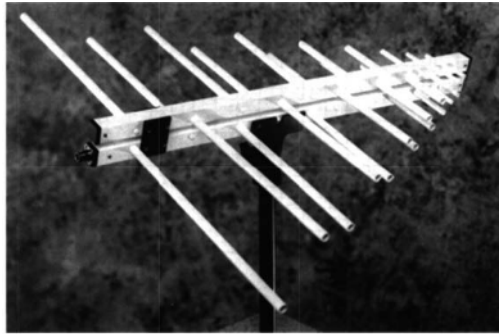


Figure 1.42. Biconical antenna and its antenna factor curve (according to doc. EMCO)

– Band D (300–1,000 MHz): the antenna must be polarized in a plane. We use more complex antennae than the doublet, for example the log-periodic antenna, made up of coupled components, whose tuning frequencies are in a geometric progression, which gives it a large bandwidth. An example is given in Figure 1.43.



LPA-30 (3 METER CALIBRATION) TYPICAL ANTENNA FACTORS (AF) AND GAIN (G)

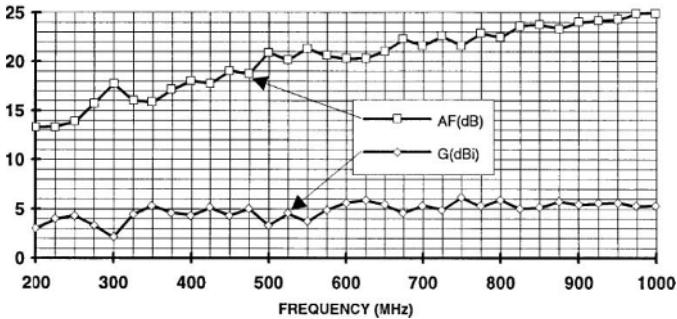


Figure 1.43. Log-periodic antenna and its antenna factor (according to doc. *Electro-Metrics*)

The positioning of the antenna is important. The measurements must be carried out away from all reflective surfaces. The height relative to the ground and the distance relative to the perturbation source must be known. The preferable distances are 3, 10, 30 m, etc. We can consult [INT 03a] for precise recommendations regarding radiated measuring techniques.

1.4.3.1. Magnetic near-field probes

When it is necessary to locally characterize an electromagnetic field close to its emission source, we are in the context of near-field measurements. For magnetic near-field measurements, there are two major types: Hall probes and loop probes.

1.4.3.2. Hall probes

The probes presented here use the Hall effect: if conductive tape is traversed by an electric current I (along the x -axis) and if a magnetic field \vec{B} is perpendicular to the plane of the tape (along the y -axis), an electric field \vec{E} appears and therefore so does a difference in potential between the edges of the tape; this phenomenon is called the Hall voltage. This voltage is oriented according to the direction perpendicular to these two axes (along the z -axis), with its orientation visible in Figure 1.44.

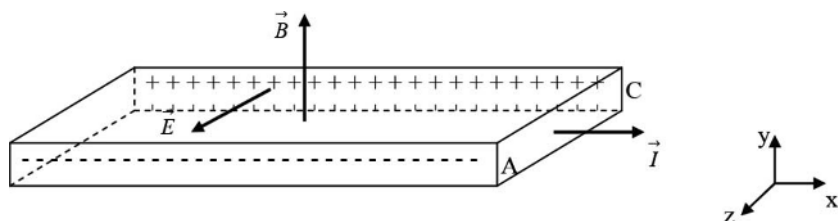


Figure 1.44. Hall probe

Hall probes help measure not only static magnetic fields, but also alternative magnetic fields up to approximately 100 kHz. Nevertheless, the Hall voltage varies with time and temperature depending on the fabrication of the probe, which requires frequent calibration. These are of a low dimension and high dynamics. They help in measuring the magnetic field within a range of 100 μT –10 T, their usage being quite restricted in EMC measurements.

1.4.3.3. Loop antennae

The magnetic field can be measured using circular or rectangular loop probes [WHI 64]. The principle of this probe rests on the immersion of a coil (one or more loops) of various forms (round, square, trapezoid, etc.) into a magnetic field. The circular probe is one of these probes. By considering a circular loop whose diameter is small compared to the wavelength, subjected to an electromagnetic plane wave where the B component is perpendicular to the plane of the loop, the E component will be in the plane of this loop. This loop is loaded by an impedance Z_c as we can see in Figure 1.45. Z_c is the impedance of the load of the measuring sensor, generally 50Ω ; we note that this connection dictates that one of the ends of the antenna must be earthed via the measuring device. This is not without consequences as we will see further on.

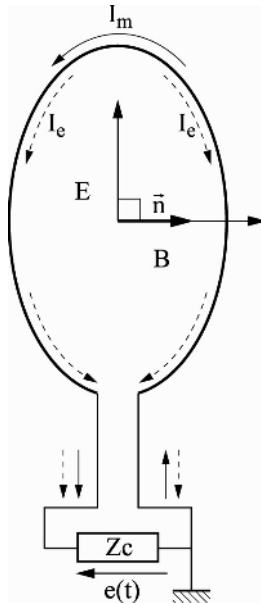


Figure 1.45. Device for measuring electromagnetic field

Each component in the field creates an EMF in the loop, where the B component induces a voltage spread around the turn; the E component induces a voltage spread in the direction of E in the plane of the loop (in accordance with Figure 1.45). The result is the circulation of two types of current I_m and I_e due, respectively, to B and E , their combined effects making up the voltage $e(t)$ at the ends of Z_c . Indeed, the connection to earth allows the circulation of a displacement current due to the vertical component E of the field in each half-branch of the loop: the loop behaves like an electric monopole, the effect of which is more sensible the higher the frequency.

A simplified electrical diagram is given in Figure 1.46 [KAN 93]. There are two electromotive forces: e_m generated by the magnetic field B and e_e generated by the magnetic field E . Each electromotive force is in series with a radiation impedance Z_{re} or Z_{rm} as well as the inductive and capacitive resistive elements in the loop: R_a , L_e , C_e , L_{a0} . The current I_a circulating in the impedance Z_c is the sum of the two currents I_e and I_m that are circulating in the electrical and the magnetic branches of the circuit, respectively.

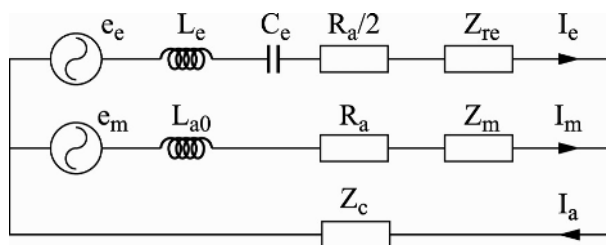


Figure 1.46. *Electrical diagram of a loop probe*

The electromotive force e_m of the magnetic side is expressed here, with A the surface and D the diameter of the turn:

$$e_m = -j2\pi fBA \quad [1.35]$$

$$e_e = \pi \frac{D}{2} E \quad [1.36]$$

L_{a0} is the low-frequency inductance of the loop and d is the diameter of the conductor making up the turn, which are expressed as:

$$L_{a0} = \mu_0 \frac{D}{2} \left(\ln \left(\frac{8D}{d} \right) - \frac{7}{4} \right) \quad [1.37]$$

The resistance R_a is the ohmic resistance of the loop, which is defined in relation to the resistivity ρ and the section s such that:

$$R_a = \frac{\rho \pi D}{s} \quad [1.38]$$

In the magnetic branch of the diagram in Figure 1.45, this resistance intervenes in its entirety, but only half in the electric branch. We note that the radiative impedance value Z_{rm} is negligible for a single-turn loop antenna [BAL 97]: for example, for a brass antenna made up of a single turn of wire with a 1 mm section and a 2 cm diameter, at 100 kHz, the value of R_a is $4.3 \times 10^{-4} \Omega$ while the value of Z_m is $3.8 \times 10^{-17} \Omega$. In practice, we can see that for $D > \lambda/10$, the electric side becomes negligible. The diameter of the probe can therefore be shaped according to the frequency range being used.

In the event that we are looking to measure only the B component of the electromagnetic field over a large frequency range (up to several tens of megahertz), it becomes necessary to shield the probe. This is achieved by winding the measuring turn(s) with a shielding that is open at the extremity opposite the measuring charge (necessary in relation to the B component), as shown in Figure 1.47. The voltage e_e is induced exclusively on the shielding and affects neither the frequencies on the turn nor the measuring impedance.

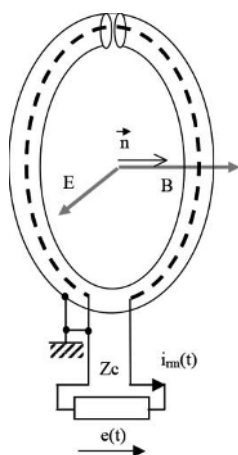


Figure 1.47. *Shielding of the measuring loop*

Thus, the shielding of the probe helps to minimize the impact of the electric field on the measurement of the magnetic field. We will therefore take note of the field probe model shown in Figure 1.48, relating to the quantities defined above.

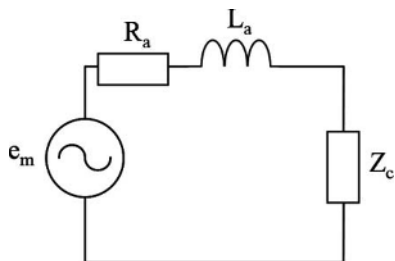


Figure 1.48. *Simplified model of a field probe*

The frequency transfer function of the probe is given as:

$$T_B(\omega) = \frac{e(\omega)}{B(\omega)} = \frac{Z_c j \omega \pi \frac{D^2}{4}}{Z_c + R_a + j \omega L_{a0}} \quad [1.39]$$

It is a high-pass function for which the chopping pulsation ω_c is given by (supposing that $Z_c = R_0 = 50 \Omega$ and that $R_0 \gg R_a$):

$$\omega_c = \frac{2R_0}{\mu_0 D \left(\log\left(\frac{8D}{d}\right) - \frac{7}{4} \right)} \quad [1.40]$$

1.4.3.3.1. Compromises on the size of the probe

If we substitute the expression of diameter D of the probe into [1.35] instead of its surface A and it is made of n turns to improve its sensitivity, we obtain:

$$e = -j2\pi f \cdot n \cdot B\pi \frac{D^2}{4} \quad [1.41]$$

The sensitivity of the probe is given by:

$$\left| \frac{e}{B} \right| = 2\pi f \pi \cdot n \frac{D^2}{4} = \pi^2 f \cdot n \frac{D^2}{2} \quad [1.42]$$

It is simpler for studying purposes to consider the spectral sensitivity, with [1.42] becoming:

$$\left| \frac{e}{Bf} \right| = \pi^2 n \frac{D^2}{2} \quad [1.43]$$

It is therefore easy to see that the bigger the diameter and number of turns, the better the sensitivity of the probe. Thus, to reduce the dimension of the antenna and obtain a more precise measurement, it is preferable to decrease its diameter; nonetheless, this results in a lower sensitivity and, if we increase the number of turns, degrades its bandwidth through the increase in parasitic capacitive effects.

Numerical Example

We wish to measure a minimum magnetic induction B of 10 nT (or 8×10^{-3} A/m) at 10 kHz. With the minimum voltage sensitivity of the measuring device being 1 μ V, we deduce that for one turn, the diameter is given by:

$$D = \frac{1}{\pi} \sqrt{\frac{2e}{nBf}} = 45 \text{ mm} \quad [1.41]$$

To illustrate this, the following table gives the characteristics of a commercial probing kit (*doc. Ets-Lindgren*). They are made up of a semi-rigid coaxial loop soldered to itself to make a turn; an opening is kept in the shielding to ensure the penetration of the field B.

Diameter	Impedance		
	R	L	Module
6 cm	237.8 m Ω	203.24 nH	12.77 Ω
3 cm	135.7 m Ω	103.1 nH	6.48 Ω
1 cm	99.46 m Ω	46.79 nH	2.94 Ω

Table 1.6. Values of parameters for the loop probes

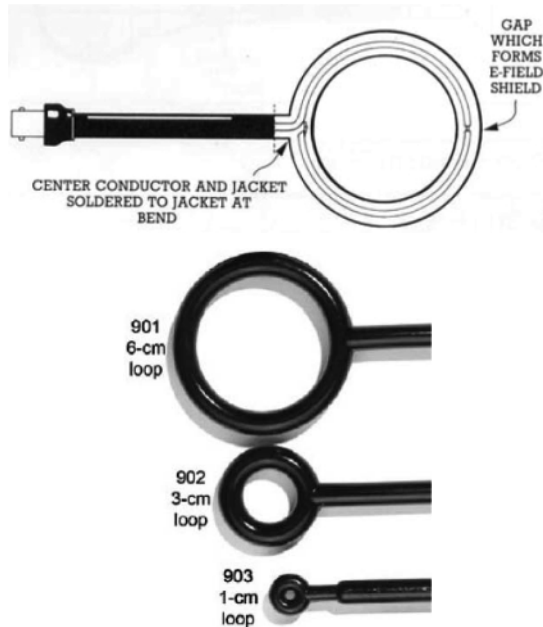
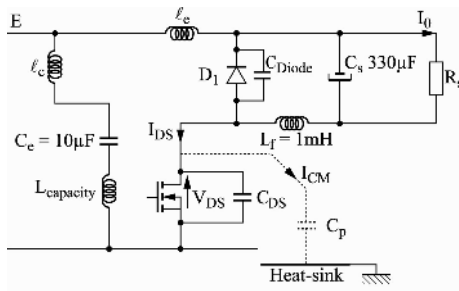


Figure 1.49. Examples of loop probes

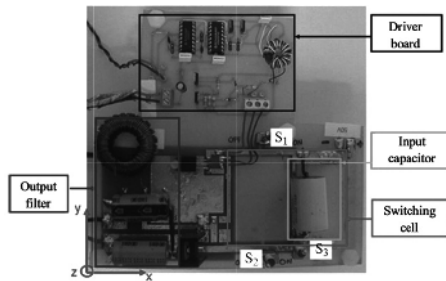
Example of application

A near-field probe can be used to create a local mapping of the field B , with this analysis helping to determine the areas where the emitted field is susceptible to perturb neighboring operations in an appliance or even to characterize the radiating circuit as an equivalent source. This is illustrated in Figure 1.51 where we have characterized through mappings of two differing frequencies the radiating H-field vertical component of the chopper represented in Figure 1.50. The measurement was made at switching frequency (20 kHz); we can clearly see the heavy radiation of the switching cell, which helps to determine its total parasitic inductance ($L_{mesh} \sim 450$ nH) by integrating the measured field over the measuring surface:

$$L_{maille} = \frac{\mu_0}{I} \iint_{surface} H_z(x, y) dx dy \tag{1.42}$$



a) Electrical diagram of a step-down chopper



b) Experimental device

Figure 1.50. Diagram and view of a chopper

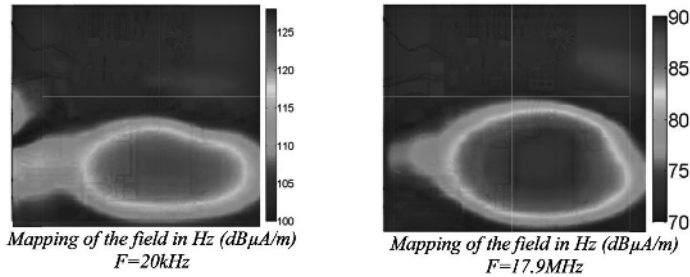


Figure 1.51. Mappings of magnetic fields near the chopper. For a color version of this figure, see www.iste.co.uk/costa/electronics.zip

We can also observe a significant radiation at 17.9 MHz but with less amplitude in the same zone due to HF resonances during switchings. The exploitation of this kind of measurement can improve the design of electronic circuits through a better understanding of the radiated effects in near-field.

1.4.4. Spectrum analyzer

This is the device that is preferably used for measurements in EMC. It is used to analyze the properties of perturbation signals or to carry out measurements while following standardized procedures. Its simplified structure is represented in Figure 1.52.

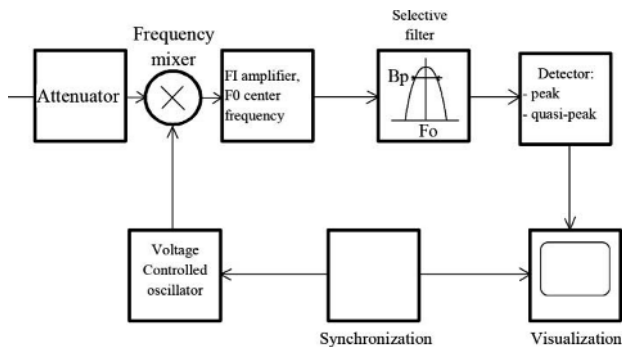


Figure 1.52. Structure of a heterodyne spectrum analyzer

The main points to consider when carrying out EMC measurements are the following:

1) *The frequency resolution*: this is the bandwidth of the analyzing filter. It ensures that measurements are made in a narrow band (only one signal harmonic in the resolution band) or large band (several signal harmonics in the bandwidth of the filter), as shown in Figure 1.54 for the case of a repeating perturbation signal, thus having a peak spectrum. The narrower the bandwidth of the filter is, the longer the measurement time will be, and the signal-to-noise ratio (S/N) will be greater. Thus, the sweeping speed v (in ms/cycle) is determined through the expression:

$$v \leq B_p^2 B_p \text{ is the bandwidth at } -6 \text{ dB of the analytical filter.}$$

The choice of the resolution bandwidth (RBW) also affects the S/N of the measurement, which increases by 10 dB when the RBW decreases by a factor of 10, as seen in Figure 1.53.

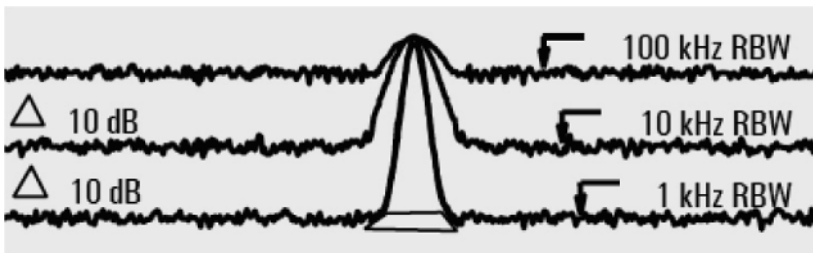


Figure 1.53. Evolution of the signal / noise resolution as a function of the resolution bandwidth of the analyzing filter

Impulsive or very low-recurrence signals are always measured in large band. Standards define the resolution according to the measured frequency band, as shown in Table 1.7.

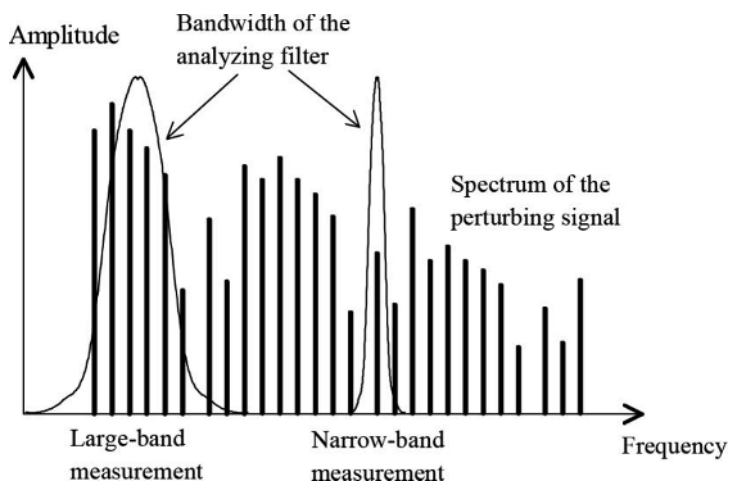


Figure 1.54. Signal measured in narrow band and large band

Frequency range	A	B	C and D
Bandwidth (-6 dB)	200 Hz	9 kHz	120 kHz

Table 1.7. Standardized resolution bandwidths for EMC measurements

2) *Input attenuator and mixer*: the mixer is a nonlinear device that introduces two kinds of errors on the display:

i) Its gain decreases when the amplitude of the signal increases (compression). This error is observable by adjusting the input attenuator upwards until we can read a level that is unrelated.

ii) It introduces distortion; the makers distinguished second- and third-order harmonic levels on the output signal depending on the input level.

Figure 1.55 shows the evolution of the S/N as a function of the input power at the level of the mixer with the previously mentioned limitations. It is therefore important to adjust the input attenuator so that the measurement is carried out with the best possible S/N.

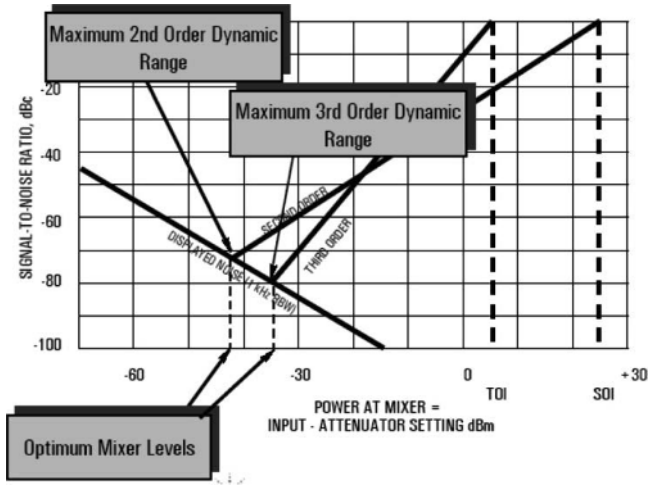


Figure 1.55. Evolution of the signal / noise ratio as a function of the input power (doc. Agilent)

Nevertheless, the attenuator introduces noise into the measurement, and the S/N degrades by 10 dB when the attenuation increases by the same amount.

3) *Detection methods:* the main detection methods are the peak, quasi-peak (QP) and average detection modes. Standards recommend QP detection as it is well adapted to the quantification of the acoustic inconvenience that results from radiofrequency perturbations.

1.4.4.1. *The QP detector*

The QP detector was introduced in the 1930s to measure the effects of interferences in the reception of signals broadcasted in amplitude modulation (AM). With a large part of these perturbations being of an impulsive nature, and with the effects of the interferences increasing with the repetition frequency, the QP detector connected to a low-frequency voltmeter ensures a measurement that is representative of the trouble of listening to the broadcast. The time constants of the QP detector were defined by

CISPR, initially for a frequency range of 150–160 kHz, which corresponds to the AM radio band, before being extended to 30 MHz⁴.

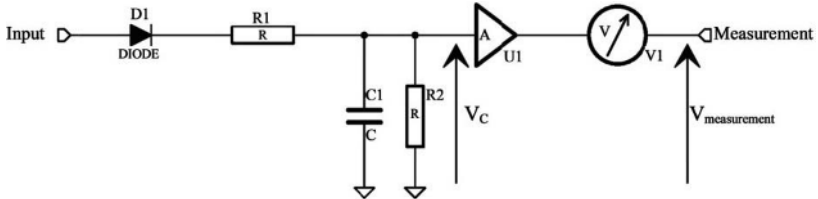


Figure 1.56. Structure of the quasi-peak detector

The structure of the QP detector is represented in Figure 1.56. The time constant is defined by $T_C = R_1 // R_2 \cdot C_1$ and the discharge time by $T_D = R_2 \cdot C_1$. The voltmeter at the output acts as second-order critical damping, the time constant of which is given in Table 1.8.

Characteristics	9–150 kHz (Band A)	150 kHz–30 MHz (Band B)	30 MHz–1 GHz (Band C)
Bandwidth of the analytical filter (–6dB)	200 Hz	9 kHz	120 kHz
Charge time (T_c) (ms)	45	1	1
Discharge time (T_d) (ms)	500	160	550
Time constant of the critical damping voltmeter (ms)	160	160	100

Table 1.8. Characteristics of the quasi-peak detector as a function of the frequency, standards CISPR 16-1-1 and ANSI C63.2

⁴ “The Quasi-Peak Detector”, by Edwin L. Bronaugh, ANSI ASC C63 Historian.

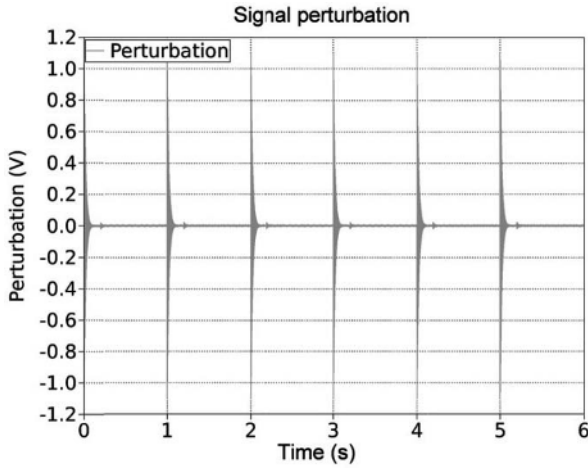


Figure 1.57. Parasitic signal, repetition frequency 1 s, analytical filter frequency 50 kHz

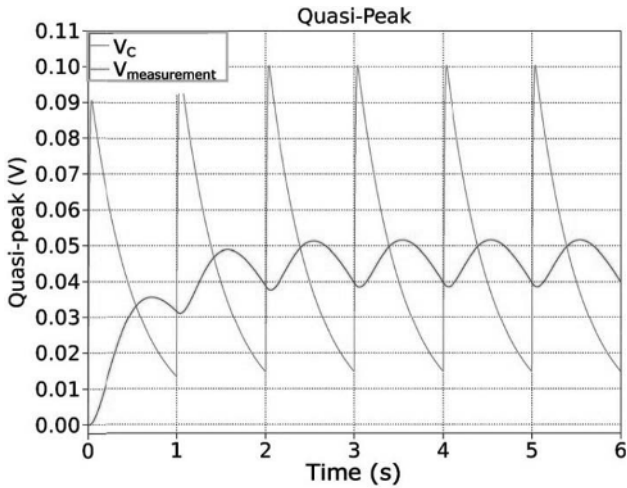


Figure 1.58. Example of band A quasi-peak detection

The output level of the QP detector varies with the frequency of the perturbation. This detection method results in much longer detection times than peak detection. The

average detection value provides a level proportional to the signal. Figure 1.59 shows the levels provided by the three detectors as a function of the perturbing signal frequency, with standardized tuning specifications.

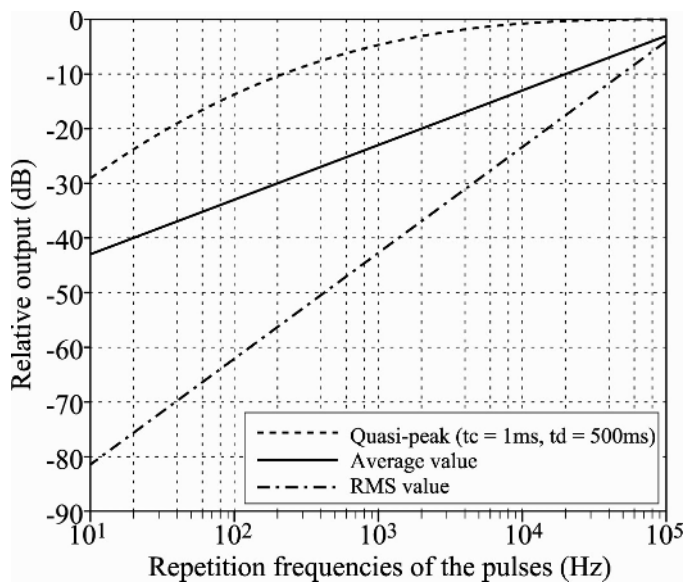


Figure 1.59. Output levels for different detectors as a function of the disruption frequency

The observations show that the measurement of a signal can vary greatly depending on whether it is in a narrow band or large band and on the detection method. A power electronic device can operate with several different switching frequencies (rectifier at 100 Hz, inverter at 20 kHz).

If the goal is to distinguish the sources of noise, spectral analysis must then be performed in narrow band with a resolution filter inferior to the lowest switching frequency. The detection method must be the peak type, as it is the quickest and best adapted.

On the other hand, if the goal is to carry out standardized measurements, the choice of the analysis method is imposed by the recommendations of CISPR. The measured levels can therefore be very different to what is observed in the previous case, and not reflect the true perturbing power of the device, as this is particularly overestimated if the measurements are performed in large band.

1.5. The standards

Two main standards categories exist: those that define the tolerated levels of radiated or conducted emissions and those that define the electromagnetic susceptibility of an appliance, namely its tolerance to electromagnetic strikes. The main objective of these standards is to outline as precisely as possible the conducted or radiated measuring environment (measuring in free space, in an anechoic chamber, support for appliances), the measuring conditions (cable lengths, distance of the antennae, height, angle, etc.), the calibration and tuning of the measuring devices being used, all with the goal of carrying out easily reproduced and reliable measurements. Since January 1, 1996, all electrical equipment have had to conform to one or more EMC standards within its category. Traditionally, the standards were established for the protection of broadcasting [COO 79]; however, this field has now expanded as the susceptibility standards can testify [INT 03b]: resistance of a particular equipment category to electrostatic discharges, to induced currents, to electromagnetic fields, to nuclear EMP (electromagnetic pulse). We will end here by mentioning emission standards concerning equipment using static converters. Table 1.9 summarizes the main standards. We must take into account that the last line corresponds to grid harmonics, which fall into the category of low-frequency perturbations conducted in power networks.

European reference	Field of application	International standard
EN 55011	Measuring methods and limits for electromagnetic perturbations in industrial and scientific appliances and medical electric radio frequency equipment.	CISPR 11
EN 55014	Measuring methods and limits for electromagnetic perturbations in electric household appliances and electric portable equipment, related to radio frequencies.	CISPR 14
EN 55015	Measuring methods and limits for electromagnetic perturbations in fluorescent lamps and electric lighting, related to radio frequencies.	CISPR 15
EN 55022	Measuring methods and limits for radio frequency perturbations in information processing machines.	CISPR 22
EN 61000-2-3	Harmonic perturbations produced in power-supply networks by electric household appliances.	IEC 61000-2-3

Table 1.9. *Major standards involving static converters*

1.6. Bibliography

- [BAL 97] BALANIS C.A., *Antenna Theory – Analysis and Design*, 2nd ed., John Wiley and Sons, Hoboken, 1997.
- [COO 79] COOK J.H., “Quasi-peak-to-RMS voltage conversion”, *IEEE Transactions on Electromagnetic Compatibility*, vol. EMC-21, no. 1, pp. 2–9, February 1979.
- [GUE 02] GUENA A., COSTA F., LABARRE C., GAUTIER C., “Unified technique in power electronics: the thin wire method”, *4th International Conference on Computation in Electromagnetics (CEM 2002)*, Bournemouth, UK, 2002.
- [INT 03a] INTERNATIONAL SPECIAL COMMITTEE ON RADIO INTERFERENCE, “CISPR 16-1, Specification for radio disturbance and immunity measuring apparatus and method”, Commission, 2003.

- [INT 03b] INTERNATIONAL SPECIAL COMMITTEE ON RADIO INTERFERENCE, "CISPR 16-2, Specification for radio disturbance and immunity measuring apparatus and method", Commission, 2003.
- [KAN 93] KANDA M., "Standard probes for electromagnetic field measurements," *IEEE Transactions on Antennas and Propagation*, vol. 41, no. 10, pp. 1349–1364, 1993.
- [KIN 82] KING RONOLD W.P., "The cylindrical dipole as a sensor or probe", *IEEE Transactions on Electromagnetic Compatibility*, vol. Emc-24, no. 3, pp. 364–367, August 1982.
- [PAU 92] PAUL C.R., *Introduction to Electromagnetic Compatibility*, Wiley Interscience, 1992.
- [UMA 87] UMAN M.A., *The Lightning Discharge*, vol. 39 of the International Geophysics Series, Academic Press, Orlando, FL, 1987.
- [WHI 64] WHITESIDE H., KING R., "The loop antenna as a probe," *IEEE Transactions on Antennas and Propagation*, vol. 12, no. 3, pp. 291–297, May 1964.